Bioorganic & Medicinal Chemistry 18 (2010) 1482–1496

Contents lists available at ScienceDirect

Bioorganic & Medicinal Chemistry

journal homepage: www.elsevier.com/locate/bmc

Synthesis, structure–activity relationship and crystallographic studies of 3-substituted indolin-2-one RET inhibitors

Luca Mologni [a,*], Roberta Rostagno [a], Stefania Brussolo [b], Phillip P. Knowles [c], Svend Kjaer [c], Judith Murray-Rust [c], Enrico Rosso [b,d], Alfonso Zambon [b,†], Leonardo Scapozza [d], Neil Q. McDonald [c], Vittorio Lucchini [b], Carlo Gambacorti-Passerini [a]

[a] Department of Clinical Medicine and Prevention, University of Milano-Bicocca, via Cadore 48, 20052 Monza, Italy
[b] Department of Environmental Sciences, University of Ca' Foscari, Venezia, Italy
[c] Structural Biology Laboratory, Cancer Research UK, London Research Institute, London, UK
[d] School of Pharmaceutical Sciences, University of Geneva, Geneva, Switzerland

ARTICLE INFO

Article history:
Received 28 September 2009
Revised 5 January 2010
Accepted 6 January 2010
Available online 11 January 2010

Keywords:
RET
Kinase inhibitor
Crystal structure
QSAR

ABSTRACT

The synthesis, structure–activity relationships (SAR) and structural data of a series of indolin-2-one inhibitors of RET tyrosine kinase are described. These compounds were designed to explore the available space around the indolinone scaffold within RET active site. Several substitutions at different positions were tested and biochemical data were used to draw a molecular model of steric and electrostatic interactions, which can be applied to design more potent and selective RET inhibitors. The crystal structures of RET kinase domain in complex with three inhibitors were solved. All three compounds bound in the ATP pocket and formed two hydrogen bonds with the kinase hinge region. Crystallographic analysis confirmed predictions from molecular modelling and helped refine SAR results. These data provide important information for the development of indolinone inhibitors for the treatment of RET-driven cancers.

1. Introduction

RET (REarranged during Transfection) is a transmembrane tyrosine kinase receptor essential for development of the sympathetic, parasympathetic and enteric nervous systems and of the kidney.[1] Its extracellular portion is composed of four cadherin-like domains, a calcium binding site and a cysteine-rich domain; the intracellular portion is a typical tyrosine kinase (TK) domain. RET is a component of a signalling system for GDNF-family ligands, and its tyrosine kinase function is thought to be activated by trans-phosphorylation events which follow ligand-induced receptor dimerization. Under physiological conditions, the formation of a complex with the ligand and a co-receptor (GFRα1–4) is needed to trigger RET kinase activity. When deregulated, RET becomes a potent oncogene. Oncogenic conversion can occur through either genomic rearrangements or germline point mutations. Depending on the type of mutations, RET induces different types of tumor. Germline point mutations cause three hereditary cancer syndromes: Multiple Endocrine Neoplasia type 2A (MEN2A), MEN2B, and Familial Medullary Thyroid Carcinoma (FMTC). Point mutations are localized either in the extracellular cysteine-rich domain, leading to constitutive ligand-independent receptor dimerization, or in the intracellular tyrosine kinase domain, causing constitutive activation of the enzyme, independently of its dimerization.[1] Papillary Thyroid Carcinoma (PTC), representing 80–90% of thyroid carcinomas, is characterized by a genomic rearrangement (a chromosomal inversion or translocation) in which the sequence of RET gene encoding for the kinase domain fuses with portions of other genes generating RET/PTC oncogenes. In such oncogenes, the catalytic domain of RET is normally fused to the N-terminal region of proteins which homodimerize in a ligand-independent manner, so that the resulting oncogenic fusion protein is activated by constitutive dimerization.[1,2] The importance of the biological processes in which RET is involved and the large variety of tumors caused by its deregulation make RET a prime target for therapeutic intervention.

Small-molecule inhibitors of oncogenic protein kinases represent an important strategy for anticancer therapy. These molecules usually compete with ATP for binding in the enzyme active site and prevent phosphate transfer from ATP to the appropriate residue (Tyr, Ser, Thr), thus blocking auto- and substrate phosphorylation and therefore signal transduction and oncogenic activity. Small molecules, belonging to several chemical classes have been shown to inhibit the oncogenic activity of RET:[1] two pyrazolo-pyrimidine derivatives, PP1 and PP2; the indolocarbazoles CEP-701 and CEP-751; SU11248 and RPI-1, two 2-indolinone derivatives; and

* Corresponding author.
E-mail address: luca.mologni@unimib.it (L. Mologni).
† Present address: The Institute of Cancer Research, London, UK.

0968-0896/$ - see front matter © 2010 Elsevier Ltd. All rights reserved.
doi:10.1016/j.bmc.2010.01.011

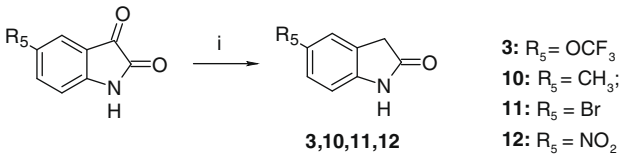

Scheme 1. Preparation of 5-substituted-indolin-2-ones from 5-substituted isatins. Reagents and conditions: (i) $NH_2NH_2H_2O$, 140 °C, 4 h, ice water, pH 2, rt, 2 days.

ZD6474, a 4-anilinoquinazoline. Among these inhibitors, ZD6474 (Vandetanib, Zactima™) is the most promising and is undergoing phase II clinical trials.[3]

We previously described nanomolar anti-RET activity of five small molecules belonging to different classes of kinase inhibitors: PD173955 (a pyrido-[2,3-*d*]pyrimidine), AG1478 (a quinazoline) and three compounds belonging to the 2-indolinone scaffold.[4,5] In particular, we studied more in depth the activity of the indolinone compound SU5416, which potently inhibited RET in vitro and in vivo.[5] These results suggested that quinazolines and indolinones could represent potential lead structures of RET inhibitors. Recently, we solved the crystal structure of the RET-ZD6474 complex;[6] as expected, the planar quinazoline structure binds in the ATP binding site and occupies the position of the adenine of ATP. Similarly, 2-indolinone derivatives have been shown to bind in the ATP site of FGFR.[7] Sun et al.[8] studied the structure–activity relationship (SAR) of a large panel of 3-substituted indolin-2-one compounds against various tyrosine kinases, showing the importance of substituents around the 2-indolinone core for potency and specificity. Rizzi et al.[9] reported the activity of a small series of 2-indolinone compounds on RET kinase. According to their findings, 5,6-dimethoxyindolinone derivatives should be favoured as RET inhibitors.

Although the 2-indolinone structure appears as a promising scaffold for the design of potent RET inhibitors, an accurate and extensive structure–activity relationship analysis has not been attempted thus far. In the present work, we designed and studied a set of novel 3-substituted indolin-2-one derivatives as potential RET inhibitors. In addition, nine commercially available compounds were included in our analysis. The inhibitors were tested to determine biochemical activity against RET, ALK, ABL and FLT3 kinases. Cellular activity was studied in RET-transformed and in non-transformed cells. Using biochemical data, the compounds were subjected to QSAR analysis. Finally, the crystal structures of three RET-ligand complexes were solved.

2. Chemistry

5-Substituted indolin-2-one compounds **3** and **10–12** were obtained by reduction of the corresponding 5-substituted isatins (indoline-2,3-dione) with hydrazine hydrate (Scheme 1).[8] For the synthesis of compound **3**, the isatin was prepared from 4-trifluoromethoxy-phenylamine via Sandmeyer reaction (not shown).[10] The indolin-2-ones **8** and **9**, respectively substituted with a methoxy group at 5- and 7-position, were obtained from (3-methoxy-phenyl)-acetonitrile by electrophilic nitration and subsequent hydrolysis of the nitrile group and reduction of the corresponding carboxylic acids (Scheme 2).[11–13] Indolin-2-ones **3** and **8–12** were converted to 3-substituted indolin-2-ones **13–25** by Knoevenagel aldolic condensation, employing available aldehydes in the presence of piperidine as the base catalyst (Scheme 3).[8]

The condensed compounds **18** and **19**, with a reactive bromine at position 5, could be further derivatized by Suzuki cross-coupling with a series of boronic acids or esters (Scheme 4).[14] Compound **25** with a reactive bromine on furan ring was further derivatized, by Suzuki cross-coupling, with furan-3-ylboronic acid and thiophen-3-ylboronic acid to obtain compounds **30** and **31** (Scheme 5).

The 5-nitro-3-substituted-indolin-2-ones (**20**, **21**, **23–25** and **30**) were converted to the corresponding 5-amino-derivatives (**32–37**) by a modification of Bellamy's reduction procedure (Scheme 6).[15] Finally, the amino group of 5-amino-3-(3,5-dimetyl-1*H*-pyrrol-2-ylmethylene)-indolin-2-one **33** was converted into amide **38** by peptidic coupling[16] with 4-((4-methylpiperazin-1-yl)methyl)benzoic acid using HBTU as the coupling agent (Scheme 7). All tested compounds are reported in Table 1.

All compounds possess the 3-exocyclic double bond and may be in principle present in the *E* (the substituent points into the direction of the aromatic ring) or the *Z* configuration (into the direction of carboxylic oxygen). The two isomers were sometimes both detected into the crude product of the Knoevenagel reaction, and could be separated by flash chromatography and characterized by NMR NOESY spectroscopy. Compounds with a pyrrolic (e.g., compound **33**) or indolic (**22**) ring at position 3 revealed dipolar interactions between the H_4 proton of the oxindolic ring and the vinyl proton (as described by Sun et al.[8]) indicating a *Z* configuration. A second diagnostic feature is the intramolecular H-bond between pyrrol aminic hydrogen and the oxindole carboxylic oxygen. These features were utilized for the assignment of the *Z* configuration to all pyrrolic compounds. In compounds with the furanic ring, NOESY spectra revealed dipolar interaction of the H_4 proton of the aromatic ring with protons of the primary furane ring (compounds **25** and **36**) or with protons of the secondary furane or thiophene ring (compounds **30**, **31** and **37**). These interactions assign to these compounds the *E* configuration. This configurational preference is due to the electronic repulsion, in configuration *Z*, between the furanic and carboxylic oxygens.[8] Compounds with the *p*-anisole ring (**23** and **34**) or the *p*-*N*,*N*-diethylaniline ring (**24** and **35**) were present as both *E* and *Z* isomers. Analysis of the interconversion processes showed that the equilibrium constants are nearly unitary, suggesting a minimal energy difference between the isomers (Supplementary Table S1). In the case of the nitroderivatives **23** and **24**, the interconversion is very fast and the distribution between *Z* and *E* isomers cannot be controlled. Therefore, these substances were excluded from biochemical assays. Interconversions of the aminoderivatives **34** and **35** are 3 orders of magnitude slower (Supplementary Table S1). Thus, the *Z* and *E* isomers of **34** were isolated

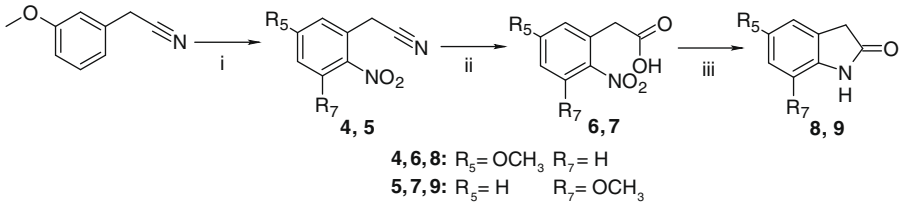

Scheme 2. Nitration of 2-(3-methoxyphenyl)acetonitrile and hydrolysis of nitrile group. Reagents and conditions: (i) CH_3COOH, acetic anhydride, HNO_3, 0 °C, 1 h; (ii) HClconcd, reflux, 3 h; (iii) Pd/C 5%, H_2, MeOH, 2 h rt.

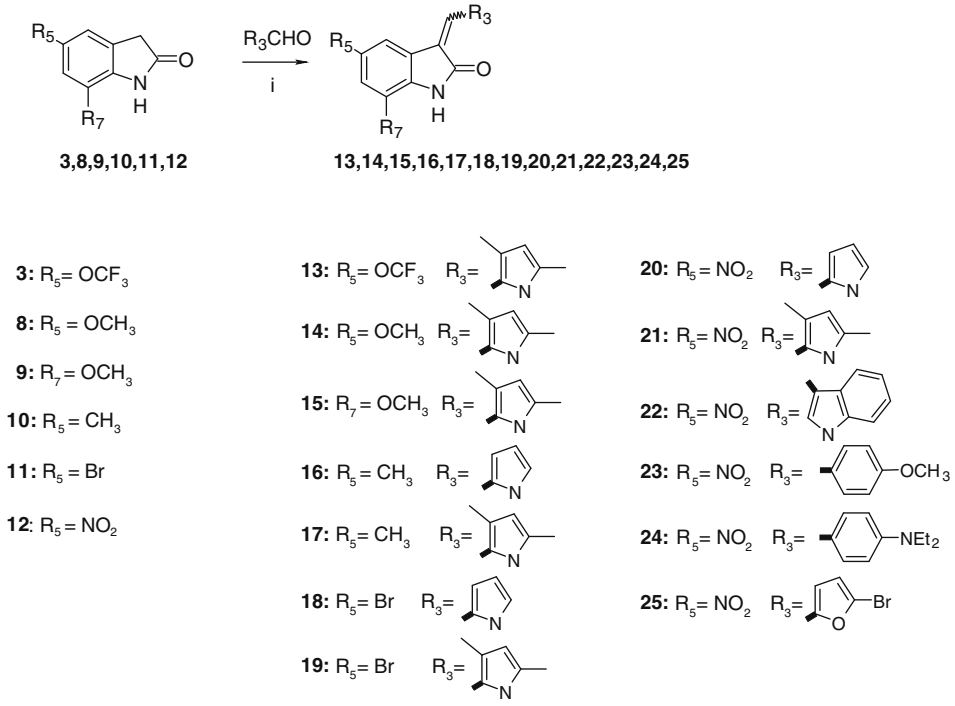

Scheme 3. Condensation of 5-substituted indolin-2-ones. R_5 and R_7 = H unless specified. Reagents and condition: (i) piperidine, EtOH, reflux 4 h.

and subjected as such to the in vitro test. Separation of the isomers of the aminoderivative **35** was unsuccessful and the compound was tested as a mixture (Table 1).

3. Results and discussion

3.1. Kinase inhibition

In order to determine inhibitory activity against RET kinase, the compounds were tested on purified recombinant RET kinase domain as described.[4] Non-linear regression of dose–response experiments allowed calculation of IC_{50} value, defined as the inhibitor concentration causing half-maximal inhibition of RET kinase activity. As shown in Table 1, most compounds having a pyrrol ring-based substituent in position 3 were good RET inhibitors, with IC_{50} values in the nanomolar to low micromolar range. Among them, inhibitors with hydrophobic (methyl/methoxy) or bulky groups in position 5 (such as **16**, **17**, **26**, **27**) tended to be less active. Interestingly, dimethyl-pyrrol almost invariably conferred higher potency than pyrrol alone (compare **17** vs **16** and **SU5416** vs **45**). It is difficult to tell whether the difference between **28** and **26** lies in the pyrrol ring or in the different position of the oxygen atom within the furan ring at position 5. Inhibitor **SU9516**, with an imidazole ring, showed comparable anti-RET activity. Notably, compounds **SU5416** and **SU11248** were previously shown to inhibit RET kinase in cells and in mice.[5,17] Compound **45** showed similar, but less specific, activity in RET-positive cells (Table 2).

Furan-substituted compounds were much less active compared to pyrrol-substituted-indolin-2-ones. One reason for their poor inhibition may be related to the predominant *E* configuration of the double bond in position 3, while most of pyrrol-substituted compounds are in the *Z* form, as described above. However, it cannot be excluded that furan may be disadvantageous in terms of interactions with the surrounding environment, compared to a pyrrol, independently of the configuration.

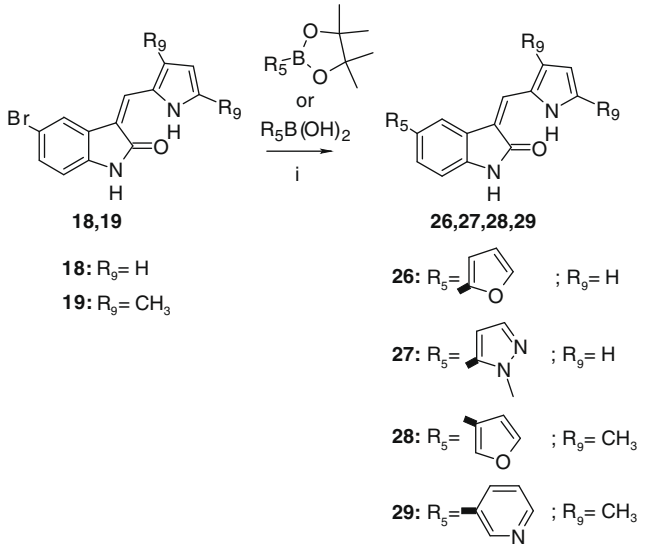

Scheme 4. Suzuki cross-coupling of 5-Br-substituted-indolin-2-one. Reagents and conditions: (i) boronic acid/ester, Na_2CO_3(satd), $Pd(PPh_3)_4$, dioxane, 110 °C, 12 h.

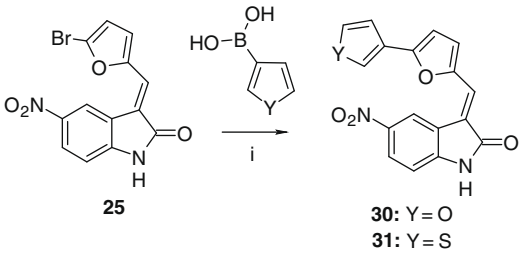

Scheme 5. Suzuki cross-coupling on 5-bromofuran group. Reagents and conditions: (i) 3-boronic acid, Na_2CO_3(satd), $Pd(PPh_3)_4$, dioxane, 110 °C, 12 h.

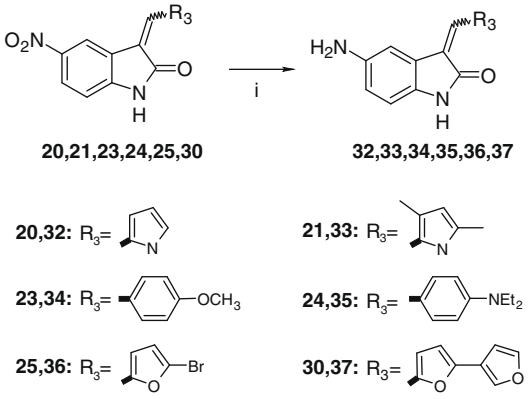

Scheme 6. Preparation of 5-amino-substituted-indolin-2-one. Reagents and conditions: (i) $SnCl_2{\cdot}2H_2O$, 1% HCl(concd), EtOH, 150 °C, 4 h.

Compounds with a phenyl ring system as the 3-substituent showed a heterogeneous behaviour. For example, the difference between **MAZ51** and **41** is striking. Again, stereochemistry may explain this apparent paradox: **MAZ51** exists predominantly as the *E* isomer on the double bond of the 3-group, because the naphthyl substituent is quite large and there is repulsion with the 2-carbonyl group. However, the presence of a methyl group in position 4 of **41** forces the naphthyl moiety to adopt the *Z* configuration, which is the more active of the two. This 4-methyl effect was not observed for **42** and **SU4984**. In this case, the substituent group in position 3 is less rigid compared to **MAZ51**/**41** and may adopt a favourable conformation more easily. Interestingly, compound **34**, which is always synthesized as a mixture of isomers, co-crystallized in the ATP pocket of RET in the *Z* form (see below), demonstrating that this is the active configuration. When the pure *Z* isomer was isolated, it showed higher potency compared to the mixture (Table 1).

To analyze specificity and cellular activity of 3-substituted indolin-2-ones, a selected subset of compounds was tested in vitro against three related tyrosine kinases, and in cell growth assays using the IL3-dependent BaF3 cell system.[4] The majority of them showed good selectivity for RET versus ALK and ABL kinases, indicating that they are not general tyrosine kinase inhibitors (Table 2). On the contrary, most compounds inhibited RET and FLT3 with similar potency. This result is not surprising, since both RET and FLT3 belong to the same structural family of the split tyrosine kinases, epitomized by VEGFR. However, there were examples of preference for RET versus FLT3: the highest selectivity was shown by compound **SU6656**, which is also a potent Src-family kinases inhibitor,[18] and therefore did not show cellular selectivity. Interestingly, compounds **29** and **VEGFR2KI-I** were potent and specific RET inhibitors both in vitro (at least with regard to the targets tested here) and in cells, respectively showing 30- and 100-fold more potent inhibition of RET-transformed BaPTC2 cells compared to parental BaF3 cells. A previous report of compound **VEGFR2KI-I** showed that it is a potent VEGFR inhibitor (IC_{50} = 70 nM), while it does not affect EGFR, IGF1R or PDGFR kinases.[8] Inhibitors that are able to block VEGFR activity in addition to the primary tumor target have gained popularity in recent years, due to the possibility of affecting tumor angiogenesis as well as tumor growth.[19] Compounds **33** and **SU11248** showed good cellular selectivity, despite lack of RET specificity versus FLT3 in vitro. **SU5416**, while showing excellent in vitro activity, was much less potent in cells, possibly due to poor solubility in cell culture medium.

3.2. Quantitative structure–activity relationship (QSAR)

QSAR analysis for RET inhibition by the indolin-2-one compounds was performed in order to correlate the biochemical data with compounds structures, and to identify positive and negative structural features within this series of compounds. The analysis was run by SYBYL v7.3 with standard parameters,[20] using the Comparative Molecular Field Analysis (CoMFA) method. Only steric and electrostatic properties of molecules were considered. Due to the limited number of ligands, it was not possible to separate the data into a training set and a test set. Because the indolin-2-one derivatives can exist as alternative isomers, it was important to establish which configuration should be used for alignment. Based on previous crystallographic studies of indolinone compounds[7,21] and our experimental data with compound **34**, it is likely that the *Z* isomer is the active form. Therefore, CoMFA analysis was run with all compounds in *Z* configuration. The activity data input were represented by Log ($1/IC_{50}$). Two alignment methods (*database* and *pharmacophoric*) were carried out. The best results were obtained using the *database* alignment and the corresponding data are summarized in Table 3. A remarkable difference between cross-validated q^2 and non cross-validated r^2 correlation coefficients was evident, indicating that the data were over-fitted, as discussed by Leach.[22] In order to overcome the over-fitting problem, an analysis of residual plot (predicted vs actual pIC_{50}) was run to identify outliers, that is, the compounds lying especially far from the diagonal.[20] Six compounds whose activity was badly predicted were eliminated (**28**, **41**, **43**, **15**, **SU6656**, **VEGFR2KI-II**) and CoMFA was repeated, yielding more consistent results (Table 3).

CoMFA analysis allowed the identification of specific features around the inhibitor scaffold, that may influence inhibitor binding. A graphical display of this analysis is depicted in Figure 1, as colour coded contours around compound **33**. Steric fields are indicated in green and yellow (Fig. 1A), with green indicating areas in which bulky groups are favoured, while yellow marks areas where bulky groups are disfavoured. The analysis suggested that bulky groups are preferred at R_3 position. In fact, pyrrol is favoured due to its interaction with the oxygen of the oxindole (**SU5416**, **32**, **33**, **45**, **29**, and **VEGFR2KI-I** all have IC_{50} <1 μM). Accordingly, compounds carrying a furan ring at that position are predicted to have negative interaction with the oxygen, and showed higher IC_{50} (**30** is the most active compound with an IC_{50} of 12 μM). On the contrary, small groups are favoured at position R_5. Consistent with this finding, compounds showing higher activity (IC_{50} <1 μM) either carry no substitution at that position, or have an amine or halogen group, with the exception of compound **29**. Compounds **26** and **27** bear bulky groups in R_5 that abrogate the effect of the pyrrol ring in

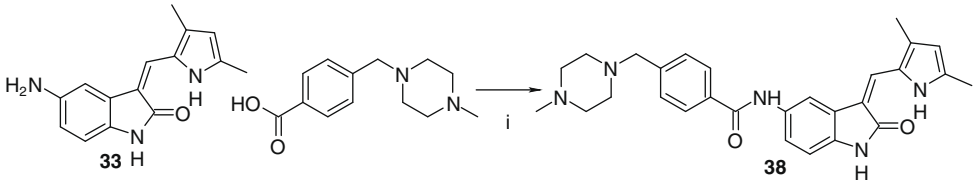

Scheme 7. Peptidic coupling. Reagents and conditions: (i) HBTU, DIEA, DMF, 12 h, rt.

Table 1
3-Substituted indolin-2-one: isomeric configurations and inhibitory activities on RET TK

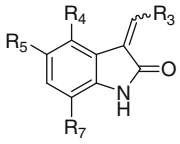

ID	R_3	R_4	R_5	R_7	Isomer	RET IC_{50} (μM)
13	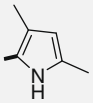	H	OCF_3	H	*Z*	2.0 ± 0.3
14	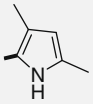	H	OCH_3	H	*Z*	4.1 ± 0.9
15	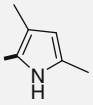	H	H	OCH_3	*Z*	5.5 ± 1.6
16		H	CH_3	H	*Z*	66 ± 10
17	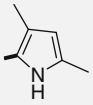	H	CH_3	H	*Z*	8.0 ±1.6
19	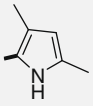	H	Br	H	*Z*	1.4 ± 0.3
22	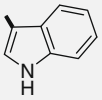	H	NO_2	H	*Z*	7.5 ± 1.3
25	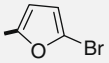	H	NO_2	H	80%*E*	22 ± 3
26		H		H	*Z*	40 ± 8
27		H		H	*Z*	20 ± 5
28		H		H	*Z*	1.1 ± 0.3
29	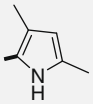	H		H	*Z*	0.58 ± 0.07
30	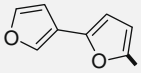	H	NO_2	H	*E*	12 ± 1
31	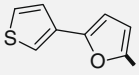	H	NO_2	H	*E*	78 ± 10
32		H	NH_2	H	*Z*	0.46 ± 0.09
33	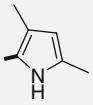	H	NH_2	H	*Z*	0.30 ± 0.04
34	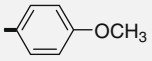	H	NH_2	H	*Z*	5.3 ± 1.3
					E	63 ± 9

Table 1 (*continued*)

ID	R_3	R_4	R_5	R_7	Isomer	RET IC_{50} (μM)
35	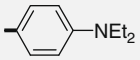	H	NH_2	H	70%*E*	1.0 ± 0.3
36	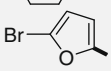	H	NH_2	H	*E*	66 ± 14
37	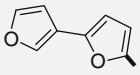	H	NH_2	H	*E*	34 ± 5
38	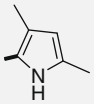	H	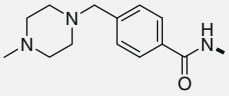	H	*Z*	5.9 ± 1.0
39	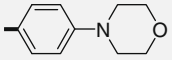	CH_3	H	H	*Z*	100 ± 4
40	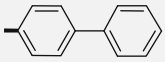	CH_3	H	H	n.d.	23 ± 3
41	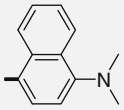	CH_3	H	H	n.d.	0.21 ± 0.03
42	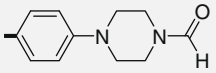	CH_3	H	H	*Z*	3.7 ± 0.5
43	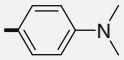	H	H	H	*Z*	>100
44	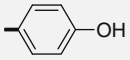	H	H	H	*E*	2.3 ± 0.4
45		H	H	H	*Z*	0.46 ± 0.04
SU5416	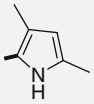	H	H	H	*Z*	0.17 ± 0.03
SU4984	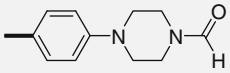	H	H	H	*E*	1.1 ± 0.2
SU6656	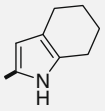	H	$SNO_2(CH_3)_2$	H	Z	0.77 ± 0.21
SU5614	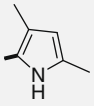	H	Cl	H	*Z*	1.0 ± 0.2
SU9516		H	OCH_3	H	*Z*	1.6 ± 0.2
SU11248	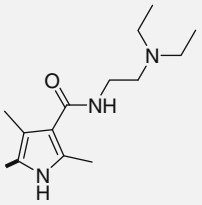	H	F	H	*Z*	1.3 ± 0.3
MAZ51	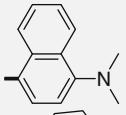	H	H	H	n.d.	45 ± 9
VEGFR2KI-II	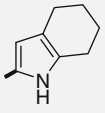	H	Br	H	Z	1.7 ± 0.3

(*continued on next page*)

Table 1 (*continued*)

ID	R_3	R_4	R_5	R_7	Isomer	RET IC_{50} (μM)
VEGFR2KI-I	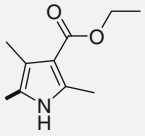	H	H	H	Z	0.76 ± 0.19

Table 2
Kinase specificity and cellular activity of selected 3-substituted indolin-2-one inhibitors

Compd	RET	ALK	ABL	FLT3	BaPTC2	BaF3
29	0.58	3.8	17	2.3	0.079	2.3
32	0.46	11	>50	2.6	0.26	0.35
33	0.30	4.8	>50	0.63	0.16	1.3
41	0.21	>50	>50	0.40	10	10
44	2.3	>50	>50	1.8	16	>50
45	0.46	>50	>50	0.35	8	17
SU5416	0.17	1.2	11	0.16	6	>50
SU6656	0.77	18	>50	8.7	0.16	0.18
SU11248	1.3	2.3	>50	0.55	0.22	1.2
VEGFR2KI-I	0.76	5.4	19	4.3	0.025	2.6

Average IC_{50} values (here reported in micromolar units) were obtained in in vitro kinase assays with four tyrosine kinases and in cell growth assays with BaF3 parental and RET-transformed (BaPTC2) cells.

Table 3
Statistical summary of QSAR-CoMFA analysis with database alignment of all compounds in *Z* configuration

Alignment	No.	r^2	q^2	*F*-values
Complete dataset	10	0.992	0.280	299.757
w/o Outliers[a]	6	0.971	0.598	132.153

[a] Outliers: **15**, **28**, **41**, **43**, **SU6656**, **VEGFR2KI-II**.
q^2: cross-validated correlation coefficient.
r^2: non-cross-validated correlation coefficient.
No.: optimum number of components.

R_3. These data also predict that there is space for substitution in position 6. Interestingly, RPI-1, an indolinone compound previously characterized as a RET inhibitor,[23] has a methoxyl group at R_6, confirming that it should be possible to build on this position.

Electrostatic fields are shown as red and blue contours in Figure 1B: red indicates areas in which negative charges are favoured and blue indicates areas in which negative charges are disfavoured. This analysis suggested that less electronegative groups are favoured near R_5: accordingly, **SU11248** and **13**, carrying a fluorine and a difluoromethoxy group, respectively, showed lower activity compared to **SU5416** (with a chlorine atom in R_5), **32** and **33** (both with an amino group) and **29** (pyridine). These observations will help design new inhibitors with improved inhibitory activity.

3.3. X-ray crystallographic analysis

Three compounds were selected for structural studies, based on their structure and biochemical activity. The aim of this analysis was to confirm and extend previous QSAR analyses. **SU5416** and **33** were among the most potent inhibitors in kinase assays. Compound **34** was chosen as a representative of compounds with a phenyl ring at position R_3 and because it is likely to be a mixture of isomers during the crystallization process. Therefore, we could conclusively determine which of the two isomers is the actual ligand. The crystal structures for the phosphorylated RET kinase domain (RET-KD-P) in complex with inhibitors **SU5416**, **33** and **34** were solved and refined at resolutions of 2.5, 2.6 and 2.0 Å, respectively (Table 4). In all three, the kinase domain forms the same 'head-to-tail' dimer as found previously;[6] the complexes of **33** and **34** crystallized in space group C2, and thus the dimer is formed by crystallographic symmetry, while for **SU5416** in P1, the two protomers are related by a non-crystallographic twofold axis.

Superpositions based on the C-lobes of RET-KD-P from the three complexes show very similar orientations of the N-lobes, and within the N-lobes the extremity of the nucleotide binding loop (residues 733–735) is disordered/poorly defined in each case. The activation loops resemble those in previous RET-KD-P structures (e.g., PDB codes 2ivt, 2ivu); each molecule shows clear electron density for pTyr905, but no side chain density for Tyr900, and therefore no indication of its phosphorylation state. The side chain of Glu775 from the C-helix forms a hydrogen bond to the active

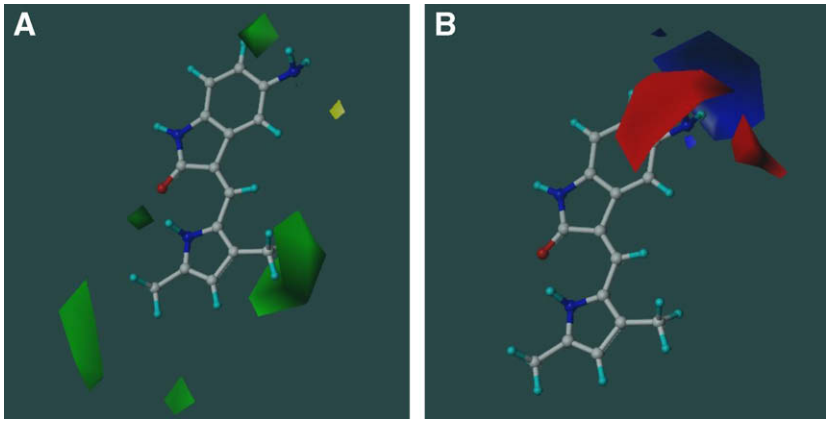

Figure 1. Contour plots for the best CoMFA model around compound **33**. Contours volumes were fixed at 80% for favoured and 20% for disfavoured levels for all fields. (A) Steric field: green indicates areas in which bulky groups are favoured, yellow indicates areas in which bulky groups are disfavoured. (B) Electrostatic field: red indicates areas in which negative charges are favoured and blue indicates areas in which negative charges are disfavoured.

Table 4
Data collection and refinement statistics for **RET/SU5416**, **RET/33** and **RET/34** complexes

Data collection			
Ligand	SU5416	33	34
Date	030807	290707	270607
Short code	SU5416	AM01	AM07
Spacegroup	$P\bar{1}$	$C2$	$C2$
Cell a, b, c (Å)	50.70, 50.76, 74.59	71.60, 70.91, 78.87	71.99, 70.68, 71.57
Cell α, β, γ (°)	103.50, 99.66,89.92	90, 101.68, 90	90, 110.35, 90
Z_A	2	1	1
Resolution (Å)	19–2.5 (2.56–2.50)	21.6–2.6 (2.74–2.60)	67–2.00 (2.11–2.00)
Beamline	In-house	In-house	ESRF ID14-1
Wavelength (Å)	1.5418	1.5418	0.9340
Detector	mar345 image plate	mar345 image plate	ADSC Q210 CCD
Unique reflections	23,524	11,886	20,421
Average redundancy	2.2 (2.2)	3.1 (3.0)	3.5 (2.3)
Completeness	95.4 (93.9)	99.1 (100)	89.5 (54.6)
R_{merge}[a] (%)	4.4 (11.3)	5.9 (23.2)	6.2 (50.7)
$R_{p.i.m.}$[b] (%)	3.9 (10.2)	4.0 (15.7)	3.7 (41.6)
$I/\sigma(I)$[c]	16.6 (6.1)	17.0 (5.2)	13.4 (2.1)
Wilson B	48	48	30
Refinement			
Resolution (Å)	30.0–2.50 (2.56–2.50)	30.00–2.60 (2.67–2.60)	67–2.0 (2.05–2.00)
R_{work} (%)	20.5 (31.8)	19.1 (27.0)	21.6 (29.9)
R_{free} (%)	24.4 (31.2)	25.6 (35.9)	27.5 (31.9)
Number of atoms (protein, ligand, water)	4327, 36, 46	2239, 19, 29	2224, 20, 71
Average B-factors (protein, ligands, water)	30, 26, 26	41, 47, 35	39, 45, 38
rms deviation bonds (Å), angles (°)	0.022, 2.4	0.016, 1.6	0.016, 1.6
Ramachandran plot % allowed, generous, disallowed	95, 4, 1	95, 4, 1	94, 5, 1

[a] $R_{merge} = \Sigma_h\Sigma_i |I(h,i) - \langle I(h)\rangle|/\Sigma_h\Sigma_i\langle I(h)\rangle$ where $I(h,i)$ is the intensity value of the i-th measurement of reflection h.
[b] $R_{p.i.m.} = \Sigma_h(1/(nh-1)\ \Sigma_i\ |I(h,i) - \langle I(h)\rangle|/\Sigma_h\Sigma_i$, where nh is the number of observations of reflection h.
[c] $I/\sigma(I)$ = Mean $(I)/\sigma(I)$.

site lysine 758. The Glu775 side chain also contacts a water molecule in the inner cavity in **SU5416** and **34**, but there is no equivalent electron density for this water molecule in **33**. This water molecule also interacts with the main chain nitrogen atom of Asp892 (from the DFG motif). The side chain of Asp892 tends to be disordered; it has been modelled as a single conformer in **34**, dual conformer in **33** and truncated at C_β in **SU5416**. The position of the side chain of Glu805 (from the linker region) allows interaction with main chain nitrogen atoms of 789 and 889—interactions that were disrupted when the larger inhibitor ZD6474 was bound (see PDB code 2ivu).

As anticipated, all three inhibitors bind in the nucleotide binding site (Fig. 2). Compound **34** was crystallized in its *Z* configuration, confirming this as the actual ligand. The three compounds form hydrogen bonds to main chain atoms of the hinge/linker region of the kinase (O805 and N807). Refined values for these distances are as follows: N–O805 is 2.80 Å for **SU5416**, 3.07 Å for **33** and 3.00 Å for **34**; O–N807 is 2.89 Å for **SU5416**, 3.12 Å for **33** and 2.77 Å for **34**. In **33** and **34**, the 5-NH_2 substituent makes a long contact to a side chain oxygen atom of Asp892 (3.03 Å in **33**, 3.33 Å in **34**). Hydrogen bonding to the hinge region conforms to the canonical pattern, mimicking interactions established by ATP with tyrosine kinases.[24] The same hydrogen bonds were described in previous studies with indolinone compounds SU5402 and SU4984 in complex with FGFR1[7] and in our RET:PP1 co-crystal structure.[6] While all three inhibitors bind in the ATP site, there are minor differences in orientation, as shown in Figure 3. Compounds **33** and **SU5416** might be expected to have their rings close to coplanar, restricted by the NH···O intramolecular hydrogen bond, while there is potential steric hindrance between the O atom and the closest $-CH_2$ of the substituted phenyl ring in **34** that might lead to out-of-plane twisting. The refinement protocol allowed for the planes of the two ring systems in each ligand to rotate with respect to each other. In **SU5416** the rings are coplanar, while in **33** and **34** there are small (ca 5°) opposite rotations of the six-membered ring (Fig. 3).

Compound **34** (the pure *Z* isomer) is approximately 1 log less active than **33** and **SU5416** (Table 1). The most obvious explanation for the observed difference in potency stems from stereochemistry: while **33** and **SU5416** are exclusively *Z* isomers, compound **34** can rapidly isomerize in solution. Therefore, even the isolated *Z* isomer will tend toward equilibrium where a significant fraction of molecules is in the inactive *E* configuration. An additional possible reason for the difference in activity is provided by crystallographic data: there is H-bonding potential between the carbonyl oxygen atom of Ala807 and the nitrogen atom of the pyrrol ring in 3-position in **33** and **SU5416**, whereas **34** has a phenyl ring here. However the N–O distances are rather long (3.5 Å in **33**, 3.3 Å in **SU5416**) and the geometry non-optimal to assign hydrogen bonds in these crystal structures. Nevertheless, the N(ligand)–O(807) interaction may be advantageous during the docking process.

Crystallographic data confirmed the conclusions from QSAR analysis with regard to steric fields around positions 3, 5 and 6 of the oxindole. In particular, the substituent in R_3 points towards the solvent and there is space for large groups, which are likely to establish favourable interactions. This feature may also be exploited to improve solubility by adding hydrophilic groups, as suggested by the increased cellular activity of **VEGFR2KI-I** compared to **SU5416**. By contrast, the amine in position R_5 of compounds **33** and **34** is in close vicinity with the surrounding pocket, as indicated by hydrogen bonding with Asp892; in addition, this 5-NH_2 group is very close to the side chain nitrogen of Lys758, although the angle is not favourable for establishing a hydrogen bond. Thus, the structural data support the conclusion that bulky substituents are not favoured in R_5. Finally, we noted that the cavity guarded by the gatekeeper residue Val804 is not occupied by the ligands; in two of them (**34** and **SU5416**) it contains water molecules, and there is certainly space for a bulkier substituent in position 6 on the indolinone ring, as anticipated by CoMFA analysis. These data will be useful to design more potent and specific inhibitors by further elaboration of this scaffold.

4. Experimental section

4.1. In vitro kinase assay

His-tagged recombinant RET, ALK, ABL and FLT3 kinase domains were expressed and purified as described.[4] Commercial inhibitors were purchased from Calbiochem (**SU5416**, **SU4984**, **SU6656**, **SU5614**, **SU9516**, **MAZ51**, **VEGFR2KI-I**, **VEGFR2KI-II**) or obtained from Pfizer, Inc. (**SU11248**). Compounds **39–45** were kindly provided by Prof. Giuseppe Zanotti (University of Padua, Italy). All inhibitors were dissolved in DMSO, aliquoted and stored at −20 °C. Upon thawing, aliquots were used immediately and never re-frozen. The ELISA-based kinase assay was performed as described.[4]

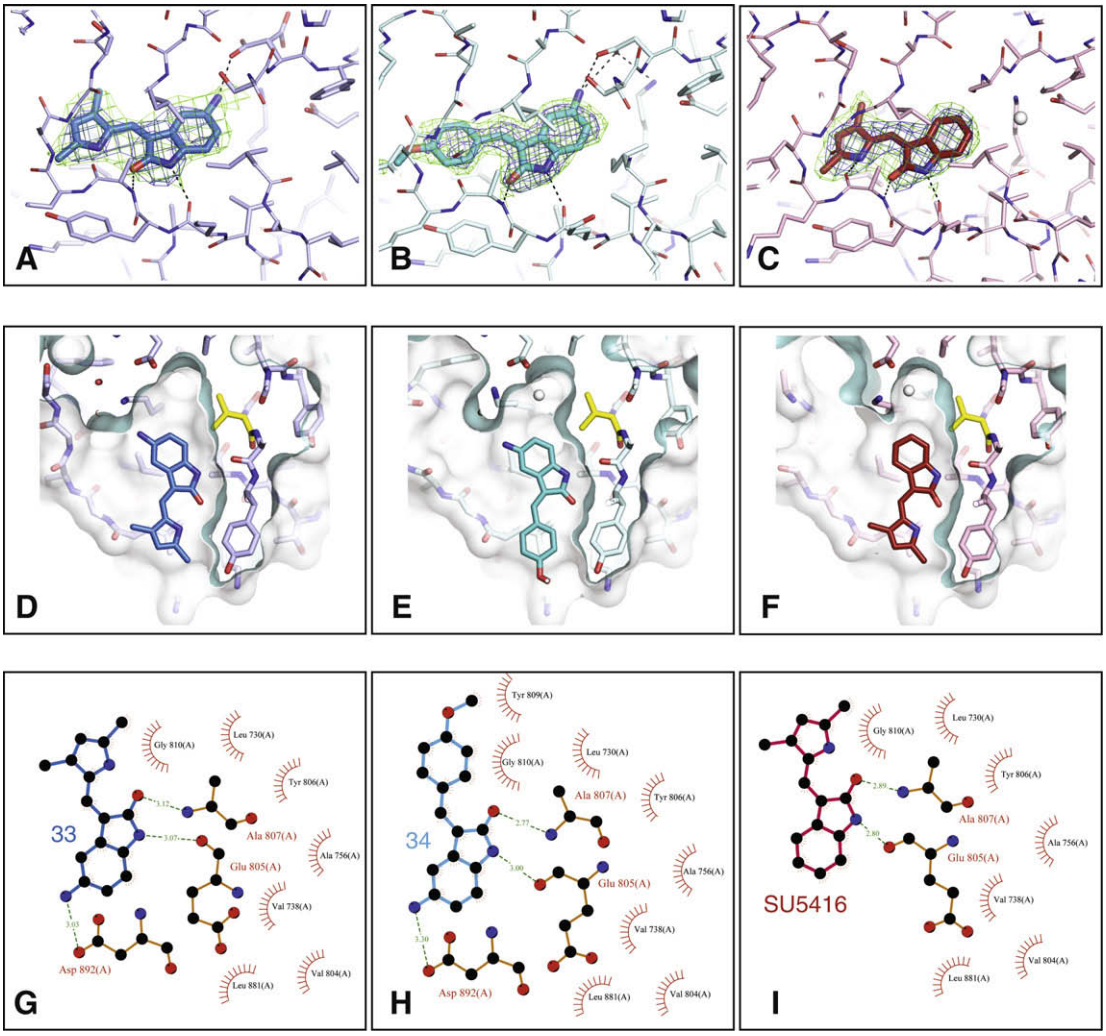

Figure 2. (A–C) Electron density for compounds **33**, **34** and **SU5416**. REFMAC-calculated electron density maps with 2mFo-DFc contoured at 1σ in green and mFo-DFc contoured at 3σ in blue; (D–F) ligand molecular surfaces of the ligand-binding pockets in RET-KD-P. The solvent side of a surface is white and the inside of a surface blue-green. Ligands are shown in stick form, with carbon atoms blue for **33**, cyan for **34** and dark red for **SU5416**. The gatekeeper Val804 side chain is highlighted in yellow. (G–I) Ligplot schematic diagrams of inhibitor–protein interactions.

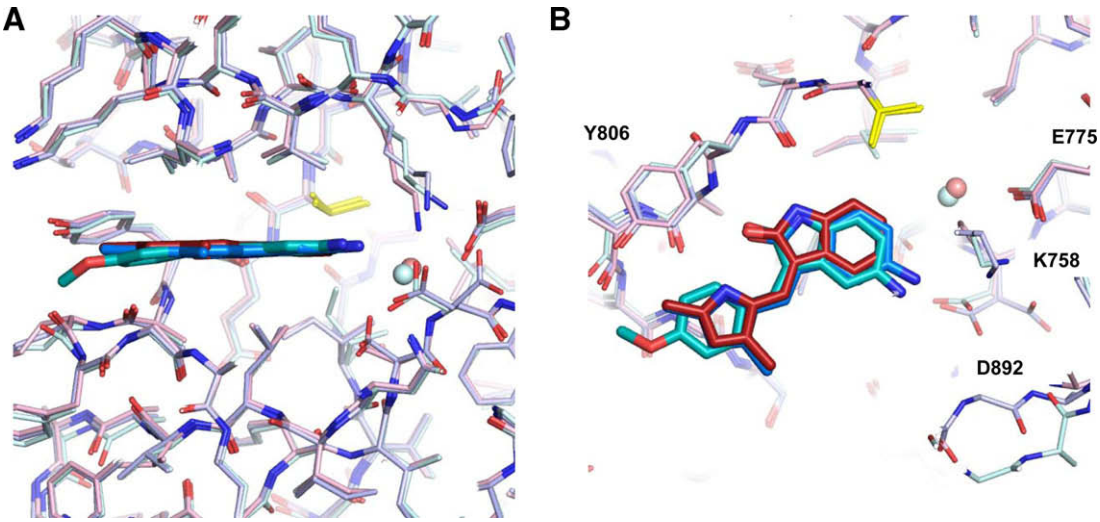

Figure 3. Superposition of **33**, **34** and **SU5416** complexes: lateral view (A) and view from the N-lobe (B). The RET-KD-P proteins were superimposed using C_α atoms from the C-lobe. Inhibitor carbon atoms are shown in blue for **33**, cyan for **34** and red for **SU5416**, and the respective protein atoms in pale shades of these colours. The gatekeeper Val804 side chain is highlighted in yellow. Water molecules in the inner cavity are shown as spheres, cyan for **34** and pink for **SU5416**.

4.2. Cell growth assay

BaPTC2 cells expressing the RET/PTC2 fusion oncogene were grown as described.[4] Proliferation assays were set up in 96-well format incubating 10^4 cells per well with increasing concentrations of inhibitor, for 72 h. During the last 8 h, the cells were pulsed with ^{3}H-thymidine (1 μCi/well) and then harvested onto a glass fibre filter. Cell-associated radioactivity was measured by liquid scintillation using a MicroBeta TriLux counter (Wallac). Each data point was done in triplicate.

4.3. QSAR analysis

Computation of steric and electrostatic fields were based on Lennard-Jones and Coulomb potentials, respectively. All molecules were charged and aligned according to SU5416 structure, using the indole core as a template; a grid (with a default 2 Å spacing, covering all the aligned molecules and extending beyond them by 4 Å in all directions) was created automatically. Steric and electrostatic properties were calculated using as probe a carbon sp3 atom with a +1 charge. Steric and electrostatic fields were scaled with a default cut-off energy of 30 kcal/mol.[20] Molecules preparation for QSAR were performed by SYBYL v7.3; the design step was performed by the Sketch option; minimization was performed using standard Tripos force fields, using steepest descents as the first method and conjugate gradients as the second one, 1000 iterations and a convergence criterion of 0.05 kcal/mol * A. Finally, Gasteiger–Marsilii charges were added to molecules.

For CoMFA studies, the Partial Least Square (PLS) analysis was initially performed with leave-one-out cross-validation and a column filtering of 1.0 kcal/mol or SAMPLS method, as indicated by SYBYL-QSAR tutorials[20] in order to determine the cross-validated correlation coefficient q^2 and the optimum number of components to build the model. Finally, a non cross-validated PLS was performed with the optimum number of component obtained from the previous calculation and with a column filtering of 1.0 kcal/mol, yielding the correlation coefficient r^2.

CoMFA contour maps were generated as the scalar product of coefficients and standard deviation (stdev * coeff) and volume of contours were fixed in 80% for favoured and 20% for disfavoured levels for all fields.

4.4. Production of RET-KD-P:inhibitor crystals

GST-tagged recombinant RET kinase domain RET-KD (residues 705–1013) was expressed in *Sf*9 cells as described previously.[6] Inhibitors were introduced into the protein solution prior to removal of the GST tag as follows. A pellet from 1.5 l of insect cells was purified by incubation with glutathione sepharose 4B beads (Amersham Bioscience) for 2 h at 4 °C. The gel was washed to remove unbound material and then incubated with 2.5 mM ATP and 5 mM magnesium sulfate for 2 h at room temperature. 10 μl of stock inhibitor (10 mg/ml in DMSO) was added to 1 ml total volume of glutathione sepharose suspension and incubated at 4 °C for 1 h. The gel was washed with Buffer A (20 mM Tris pH 8, 100 mM NaCl, 1 mM DTT and 1 mM EDTA), and then treated with GST-linked 3C protease (PreScission protease, Amersham Bioscience) overnight at 4 °C. Protein–inhibitor complexes were concentrated to 4.5 mg/ml in buffer A.

Crystals were grown at 16 °C in sitting drops containing 2 μl of protein solution and 2 μl of reservoir solution (reservoir volume 0.5 ml): for **33** and **34** the reservoir solution contained 1.85 M sodium formate, 0.2 M LiCl and 0.1 M sodium citrate pH 5.5; and for **SU5416** the reservoir solution contained 1.75 M sodium formate, 0.15 M potassium thiocyanate and 0.1 M sodium citrate pH 5.5. All crystals were harvested directly into the cryoprotectant *n*-paratone and flash-frozen in a dry nitrogen stream at 100 K.

4.5. Data collection and structure solution

Data were collected as shown in Table 4, integrated with the program MOSFLM[25] and processed with SCALA and TRUNCATE.[26] Structures solved by molecular replacement using MOLREP,[27] as implemented in the CCP4 Suite,[26] with a search model made from the phosphorylated RET-KD-P protein (PDB code 2ivt) with flexible regions removed. The structures were refined using REFMAC5[28] and rebuilt using Coot.[29] Other calculations were made with programs from the CCP4 Suite unless otherwise stated. The protein and more ordered water molecules were rebuilt and refined for several cycles prior to introduction of ligand into the calculation. Ligand libraries were generated with the PRODRG server.[30] Refinement statistics are given in Table 4, and coordinates and structures factors have been deposited with PDB codes 2X2K (**33** complex), 2X2L (**34** complex) and 2X2M (**SU5416** complex). Structural figures were generated with PyMOL (DeLano Scientific, South San Francisco, CA) and LIGPLOT.[31]

4.6. Chemistry

All the starting materials used for the synthesis were commercially available and used without purification; solvents and reagents were dried prior to use as required. Chromatographic purification was performed on Silica Gel 60 M, 230–400 mesh ASTM. ^{1}H and ^{13}C NMR were measured at 400 MHz and 100 MHz, respectively, in DMSO-d_6 or $CDCl_3$ with Me_4Si as the internal standard. Gas-chromatographic analyses were performed with a 30 m, 0.25 mmID, Rtx-5MS capillary columm (5:95 diphenyl-/dimethyl-polysiloxane) on a GS–MS unity. ESI-MS analyses were performed under, negative or positive ionisation mode on API 150 EX Turbo ion spray Amplied Biosistem. Mass spectra HRMS analyses were performed under ESI positive or EI ionization mode, on a QSTAR XL-MS unity.

4.6.1. NMR NOESY spectroscopy

For the *Z* isomer the diagnostic dipolar interaction is between the H_4 proton of the oxindolic ring and the vinylic H_8 proton (the adopted atom numbering is shown in Supplementary Scheme S1). In the case of the *E* isomer the H_4 proton interacts with the protons of the primary R_3 ring ortho to the junction (H_{11} in structure *a*, or H_{10}/H_{14} in structure *b*) or with the protons of the secondary ring (H_{15}/H_{17} in structure *a*).

4.6.2. Synthesis of (2)

A typical procedure for the synthesis of isatin[10] was used to prepare 2-hydroxyimino-*N*-(4-trifluoromethyl-phenyl)-acetamide (**1**). A solution of sodium sulfate (50 g) in 60 mL of water was stirred until all the solids were dissolved. A solution of 4-trifluoromethoxy-phenylamine (3.5 g, 20 mmol) in 30 mL of 1 N aqueous HCl and 6 mL of EtOH was added to the resulting aqueous solution. The mixture was stirred and chloral hydrate (3.6 g, 22 mmol) was added. A solution of hydroxylamine hydrochloride (4.6 g, 66 mmol) in 20 mL of water was then added to the solution. The final mixture was heated with stirring to a gentle reflux until the solids were dissolved, and heating was continued for an additional 15 min. The resultant solution was poured on to 300 g of ice, stirred, and the product was precipitated from solution, collected by suction filtration, washed with water and dried to give 4.5 g (90%) of (**1**): ^{1}H NMR (DMSO-d_6, 400 MHz), δ (ppm): 12.21 (br s, 1H), 10.37 (br s, 1H), 7.78 (d, 2H, J = 9.3 Hz), 7.63 (s, 1H), 7.32 (d, 2H, J = 9.0 Hz). ^{13}C NMR (DMSO-d_6, 100 MHz), δ (ppm): 161.0, 156.2, 149.9, 122.6, 121.7, 128.1, 114.5(2C). ESI-MS (*m/z*)

$[M-H]^-$, 247.1. 2-Hydroxyimino-*N*-(4-trifluoromethoxy-phenyl)-acetamide (**1**) (4 g, 16 mmol) was slowly added to 40 mL of concentrated sulphuric acid at 100 °C. The reaction mixture was heated for 1 h and the resultant solution was poured into 280 g of ice and water, stirred for 1 h and filtered. The solid was washed with water and dried to give 1.7 g (46%) of 5-trifluoromethoxy-1*H*-indole-2,3-dione (**2**): ^{1}H NMR (DMSO-d_6, 400 MHz), δ (ppm): 11.16 (br s, 1H), 7.57 (dd, 1H, J = 8.2, 2.2 Hz), 7.50 (s, 1H, J = 8.2 Hz), 6.97 (d, 1H, J = 8.2 Hz); ^{13}C NMR (DMSO-d_6, 100 MHz), δ (ppm): 188.6, 164.6, 154.6, 148.6, 136.1, 123.8, 123.0, 118.6. ESI-MS (*m/z*) $[M-H]^-$, 229.9.

4.6.2.1. (5-Methoxy-2-nitro-phenyl)-acetonitrile (4) and (3-methoxy-2-nitro-phenyl)-acetonitrile (5). A solution of (3-methoxy-phenyl)-acetonitrile (3 g, 20 mmol) in a 1:1 mixture of glacial acetic acid (23 mL) and acetic anhydride (23 mL) was cooled at 0 °C, and concentrated nitric acid (3.3 mL) was added dropwise. After 1 h water was added (20 mL) of, the precipitate was filtered and chromatographed on silica gel (90:10, *n*-Esane/AcOEt) to obtain (5-methoxy-2-nitro-phenyl)-acetonitrile **(4)** 1.2 g (32%) and (3-methoxy-2-nitro-phenyl)-acetonitrile **(5)** 0.8 g (22%), both as yellow solid. **(4):** ^{1}H NMR ($CDCl_3$, 400 MHz), δ (ppm): 8.26 (d, 1H, J = 9.1), 7.18 (d, 1H, J = 2.8), 6.98 (dd, 1H, J = 9.1, 2.8), 4.25 (s, 2H), 3.95 (s, 3H).^{13}C NMR ($CDCl_3$, 100 MHz) δ (ppm): 164.0, 140.3(2C), 128.6, 116.4, 116.3, 113.8, 56.1, 23.3. MS (EI, 70 eV) *m/z*: 177 (M^+-CH_3, 26), 149 (100), 105 (14), 76 (21). **(5)**: ^{1}H NMR ($CDCl_3$, 400 MHz), δ (ppm): 7.5 (t, 1H, J = 8.1), 7.2 (d, 1H, J = 7.8), 7.07 (d, 1H, J = 7.8), 3.92 (s, 3H), 3.77 (s, 2H). ^{13}C NMR ($CDCl_3$, 100 MHz) δ (ppm): 151.6, 132.0(2C), 123.5, 120.6, 115.6, 112.9, 56.6, 19.9. MS (EI, 70 eV) *m/z*: 177.2 (M^+-CH_3, 26), 149.2 (100), 105.2 (14), 76.2 (21).

4.6.2.2. (5-Methoxy-2-nitro-phenyl)-acetic acid (6) and (3-methoxy-2-nitro-phenyl)-acetic acid (7). A stirred solution of **(4)** or **(5)**, (42 mg, 2.1 mmol) in concentrated HCl was heated to reflux. After 3 h the mixture was cooled to 0 °C and 6 mL of ice water was added. The precipitate was filtered and dried to give the compounds in 67% yield. Compound **6** was obtain as pink solid: ^{1}H NMR (DMSO-d_6, 400 MHz), δ (ppm): 8.22 (d, 1H, J = 9.2), 6.93 (dd, 1H, J = 9.2, 2.8), 6.80 (d, 1H, J = 2.8), 4.05 (s, 2H), 3.90 (s, 3H), 1.78 (br s, 1H). ^{13}C NMR (DMSO-d_6, 100 MHz) δ (ppm): 171.2, 163.1, 141.4, 133.8, 127.5, 118.7, 113.1, 56.1, 38.9. MS (EI, 70 eV) *m/z*: 211.1 (M^+, 17), 165.1 (70), 150.1 (80), 122.1 (50), 95.1 (48), 77.1 (100), 51.1 (70). Compound **7** was obtain as yellow solid: ^{1}H NMR (DMSO-d_6, 400 MHz), δ (ppm): 7.51 (t, 1H, J = 8.4), 7.24 (d, 1H, J = 8.4), 7.04 (d, 1H, J = 8.2), 3.86 (s, 3H), 3.61 (s, 2H), 3.35 (1H, OH).^{13}C NMR (DMSO-d_6, 100 MHz) δ (ppm): 170.7, 150.6, 140.8. 131.6, 128.2, 123.5, 112.3, 56.6, 36.4. MS (EI, 70 eV) *m/z*: 211.1 (M^+, 17), 165.1 (70), 150.1 (80), 122.1 (50), 95.1 (48), 77.1 (100), 51.1 (70).

4.6.2.3. 5-Methoxy-1,3-dihydro-indol-2-one (8) and 7-methoxy-1,3-dihydro-indol-2-one (9). To a stirred solution of **(6)** or **(7)** (300 mg, 1.5 mmol) in acetic acid (4.5 mL) was added Pd/C 5% (20 mg) as catalyst, the mixture was poured under hydrogen atmosphere. After 2 h at room temperature CH_2Cl_2 (15 mL) was added, the mixture was filtered through Celite. The organic layer was concentrated and the residue was chromatographed on silica gel (80:20, *n*-hexane/AcOEt) to give **(8)** 98 mg (40%) as white solid and **(9)** 102 mg (50%) as orange solid. Compound **8**: ^{1}H NMR ($CDCl_3$, 400 MHz), δ (ppm): 8.50 (br s, 1H), 6.85 (d, 1H, J = 2.0), 6.79 (d, 1H, J = 8.4 Hz), 6.74 (dd, 1H, J = 8.0, 2.0 Hz), 3.77 (s, 3H), 3.52 (s, 2H).^{13}C NMR ($CDCl_3$, 100 MHz) δ (ppm): 177.4, 155.6, 135.8, 126.6, 112.4, 111.8, 109.9, 55.8, 36.6. MS (EI, 70 eV) *m/z*: 163.2 (M^+, 100), 148.2 (38), 134.2 (20), 107.2 (26), 106.2 (44), 92.2 (44). **(9)**: ^{1}H NMR ($CDCl_3$, 400 MHz), δ (ppm): 8.07 (br s, 1H), 6.98 (t, 1H, J = 7.7), 6.85 (d, 1H, J = 7.7 Hz), 6.81 (d, 1H, J = 7.7 Hz), 3.67 (s, 3H), 3.55 (s, 2H). ^{13}C NMR ($CDCl_3$, 100 MHz) δ (ppm): 176.5, 143.7, 131.2, 126.0, 122.7, 116.9, 110.1, 55.6, 36.7. MS (EI, 70 eV) *m/z*: 163.2 (M^+, 100), 148.2 (38), 134.2 (20), 107.2 (26), 106.2 (44), 92.2 (44).

4.6.3. General reduction procedure of 5-substituted isatin to 5-substituted-1,3-dihydro-indol-2-one

A stirred solution of 5-substituted isatin (0.1 mol) in hydrazine hydrate (60 mL) was heated to 140 °C for 4 h. The reaction mixture was cooled to room temperature, poured into 300 mL of ice water, and acidified to pH 2 with 6 N hydrochloric acid. After standing at room temperature for 2 days the precipitate was collected by vacuum filtration, washed with water, and dried under vacuum (50% yield).

4.6.3.1. 5-Trifluoromethoxy-1,3-dihydro-indol-2-one (3). Compound **3** (93% yield); ^{1}H NMR (DMSO-d_6, 400 MHz), $\delta\delta$ (ppm): 10.57 (br s, 1H), 7.22 (d, 1H, J = 2.0 Hz), 7.15 (ddquart, 1H, J = 8.4, 2.6 Hz, J_{HF} = 0.9 Hz), 6.87 (d, 1H, J = 8.4 Hz), 3.52 (s, 2H). ^{13}C NMR (DMSO-d_6, 100 MHz), δ (ppm): 176.2, 142.9, 142.8, 127.7, 120.5, 120.1 (quartet, J_{CF} = 255.0 Hz), 118.1, 109.7, 36.0. ESI-MS (*m/z*) $[M-H]^-$, 216.1.

4.6.3.2. 5-Methyl-1,3-dihydro-indol-2-one (10). Compound **10** (45% yield); ^{1}H NMR (DMSO-d_6, 400 MHz), δ (ppm): 10.24 (br s, 1H), 6.99 (s, 1H), 6.94 (d, 1H, J = 7.8 Hz), 6.67 (d, 1H, J = 7.8 Hz), 3.39 (s, 2H), 2.22 (s, 3H). ^{13}C NMR (DMSO-d_6, 100 MHz), δ (ppm): 176.3, 141.2, 129.9, 127.6, 125.8, 125.1, 108.8, 35.2, 20.6. MS (EI, 70 eV) *m/z*: 147.2 (M^+, 95), 119.2 (55), 118.2 (100).

4.6.3.3. 5-Bromo-1,3-dihydro-indol-2-one (11). Compound **11** (60% yield); ^{1}H NMR (DMSO-d_6, 400 MHz), δ (ppm): 10.48 (br s, 1H), 7.36 (s, 1H), 7.32 (d, 1H, J = 8.2 Hz), 6.73 (d, 1H, J = 8.2 Hz), 3.48 (s, 2H). ^{13}C (DMSO-d_6, 100 MHz) δ (ppm): 176.6, 140.1, 134.6, 130.7, 128.2, 124.3, 119.2, 39.6. MS (EI, 70 eV) *m/z*: 213.1 (M^+, 100), 211.1 (M^+, 100), 184.1 (65), 182.1 (65), 158.0 (15), 156.0 (15), 132.1 (25), 104 (37).

4.6.3.4. 5-Nitro-1,3-dihydro-indol-2-one (12). Compound **12** (60% yield); ^{1}H NMR (DMSO-d_6, 400 MHz), δ (ppm): 11.00 (br s, 1H), 8.13 (dd, 1H, J = 8.6, 2.4 Hz), 8.07 (d, 1H, J = 2.4 Hz), 6.88 (d, 1H, J = 8.6 Hz), 3.61 (s, 2H). ^{13}C NMR (DMSO-d_6, 100 MHz) δ (ppm): 176.6, 150.4, 141.7, 127.1, 124.9, 120.0, 109.0, 35.6. MS (EI, 70 eV) *m/z*: 178.2 (M^+, 100), 148.2 (56), 132.2 (25), 120.2 (30), 104.2 (65).

4.6.4. General procedure for 3-substituted indolin-2-one

A stirred solution of proper oxindole (1 equiv), aldehyde (1.2 equiv), and piperidine (0.1 equiv), in EtOH 10 mL/1 mmol was heated to 90 °C for 4 h. After cooling at room temperature, the precipitate was filtered, washed with cold EtOH.

We reported here the NMR chemical shift for the major isomer. Only for compounds **23, 24**, **34**, **35**, we described the NMR analytical data for both isomers.

4.6.4.1. 3-(3,5-Dimethyl-1*H*-pyrrol-2-ylmethylene)-5-trifluoromethoxy-1,3-dihydro-indol-2-one (13). Compound **13** (60% yield); ^{1}H NMR (DMSO-d_6, 400 MHz), δ (ppm): 13.41 (br s, 1H), 10.94 (br s, 1H), 7.87 (s, 1H), 7.71 (s, 1H), 6.99 (d, 1H, J = 8.0 Hz), 6.93 (d, 1H, J = 8.0 Hz), 6.02 (s, 1H), 2.16 (s, 3H), 2.10 (s, 3H). ^{13}C NMR (DMSO-d_6, 100 MHz), δ (ppm): 169.5, 147.5, 143.2, 137.1, 136.7, 133.4, 127,5, 126.9, 125.8, 118.1, 113.1, 111.8, 111.4, 110.1, 109.7, 13.6, 11.4. ESI-HRMS (*m/z*) $[M+H]^+$ calcd, 323.1001; obs, 323.0992.

4.6.4.2. 3-(3,5-Dimethyl-1*H*-pyrrol-2-ylmethylene)-5-methoxy-1,3-dihydro-indol-2-one (14). Compound **14** (50% yield); ^{1}H NMR (DMSO-d_6, 400 MHz), δ (ppm): 13.43 (br s , 1H), 10.57 (br s, 1H), 7.57 (s, 1H), 7.39 (d, 1H, J = 2.5 Hz), 6.74 (d, 1H, J = 8.4 Hz), 6.65 (dd, 1H, J = 8.4, 2.5 Hz), 5.99 (d, 1H, J = 2.5 Hz), 3.75 (s, 3H), 2.30 (s, 3H), 2.30 (s, 3H). ^{13}C NMR (DMSO-d_6, 100 MHz), δ (ppm): 169.5, 154.8, 135.6, 132.1, 131.7, 126.9, 126.6, 123.7, 113.3, 112.5, 111.9, 109.7, 104.1, 55.7, 13.5, 11.4. ESI-HRMS (m/z) $[M+H]^+$ calcd, 269.1284; obs, 269.1297.

4.6.4.3. 3-(3,5-Dimethyl-1*H*-pyrrol-2-ylmethylene)-7-methoxy-1,3-dihydro-indol-2-one (15). Compound **15** (60% yield); ^{1}H NMR (DMSO-d_6, 400 MHz), δ (ppm): 13.42 (br s, 1H), 10.81 (br s, 1H), 7.51 (s, 1H), 7.32 (d, 1H, J = 7.8 Hz), 6.92 (t, 1H, J = 7.8 Hz), 6.80 (d, 1H, J = 8.0 Hz), 5.96 (d, 1H, J = 2.5 Hz), 3.82 (s, 3H), 2.31 (s, 3H), 2.28 (s, 3H). ^{13}C NMR (DMSO-d_6, 100 MHz), δ (ppm): 169.3, 143.6, 135.7, 131.6, 126.8, 126.7, 126.6, 123.8, 121.4, 113.2, 112.5, 111.0, 108.8, 55.6, 13.5, 11.3. ESI-HRMS (m/z) $[M+H]^+$ calcd, 269.1284; obs, 269.1297.

4.6.4.4. 5-Methyl-3-(1*H*-pyrrol-2-ylmethylene)-1,3-dihydro-indol-2-one (16). Compound **16** (70% yield); ^{1}H NMR (DMSO-d_6, 400 MHz), δ (ppm): 13.31 (br s, 1H), 10.77 (br s, 1H), 7.68 (s, 1H) 7.43 (m, 1H), 7.31 (m, 1H), 6.93 (m, 1H, J = 7.8 Hz), 6.78 (m, 1H), 6.74 (d, 1H, J = 7.8 Hz), 6.32 (m, 1H), 2.27 (s, 3H). NOESY: dipolar interaction detected between H_4 (δ 7.43) and H_8 (δ 7.68). ^{13}C NMR (DMSO-d_6, 100 MHz), δ (ppm): 169.3, 136.8, 130.0, 129.6, 127.4, 126.1, 125.5, 125.2, 120.1, 119.1, 117.1, 111.4, 109.3, 20.94; ESI-HRMS (m/z) $[M+H]^+$ calcd, 225.1022; obs, 225.1014.

4.6.4.5. 3-(3,5-Dimethyl-1*H*-pyrrol-2-ylmethylene)-5-methyl-1,3-dihydro-indol-2-one (17). Compound **17** (60% yield); ^{1}H NMR (DMSO-d_6, 400 MHz), δ (ppm): 13.34 (br s, 1H), 10.65 (br s, 1H), 7.52 (d, 1H, J = 1.4 Hz), 7.50 (s, 1H), 6.88 (dd, 1H, J = 7.9, 1.6 Hz), 6.73 (d, 1H, J = 7.8 Hz), 5.97 (d, 1H, J = 2.6 Hz), 2.29 (s, 3H), 2.28 (s, 3H), 2.27 (s, 3H). ^{13}C NMR (DMSO-d_6, 100 MHz), δ (ppm): 169.5, 136.0, 135.4, 131.3, 129.6, 126.6, 125.9, 123.2, 123.1, 118.6, 118.6, 113.0, 112.4, 20.9, 13.5, 11.3; ESI-HRMS (m/z) $[M+H]^+$ calcd, 253.1335; obs, 253.1327.

4.6.4.6. 5-Bromo-3-(1*H*-pyrrol-2-ylmethylene)-1,3-dihydro-indol-2-one (18). Compound **18** (44% yield); ^{1}H NMR (DMSO-d_6, 400 MHz); signals broadened by radicals; δ (ppm): 13.27 (br s, 1H), 10.99 (br s, 1H), 7.86 (br s, 2H), 7.37 (br s, 1H), 7.25 (br s, 1H), 6.82 (br s, 2H), 6.35 (br s, 1H), ^{13}C NMR (DMSO-d_6, 100 MHz), δ (ppm): 174.1, 143.0, 134.7, 134.0, 133.2, 132.8, 131.7, 126.5, 126.4, 120.5, 118.5, 116.9, 116.5. ESI-HRMS (m/z) $[M+H]^+$ calcd, 288.9976, obs, 288.9980.

4.6.4.7. 5-Bromo-3-(3,5-dimethyl-1*H*-pyrrol-2-ylmethylene)-1,3-dihydro-indol-2-one (19). Compound **19** (50% yield); ^{1}H NMR (DMSO-d_6, 400 MHz); signals broadened by radicals; δ (ppm): 13.35 (br s, 1H), 10.87 (br s, 1H), 7.99 (br s, 1H), 7.66 (br s, 1H), 7.18 (br s, 1H), 6.79 (br s, 1H), 6.00 (br s, 1H), 2.30 (br s, 3H), 2.29 (br s, 3H), ^{13}C NMR (DMSO-d_6, 100 MHz), δ (ppm): 174.3, 142.1(2C), 138.4, 133.5, 132.7, 132.1, 130.2, 125.9, 118.3, 118.2, 116.3, 116.1, 18.7, 16.5. ESI-HRMS (m/z) $[M+H]^+$ calcd, 317.0284; obs, 317.0270.

4.6.4.8. 5-Nitro-3-(1*H*-pyrrol-2-ylmethylene)-1,3-dihydro-indol-2-one (20). Compound **20** (70% yield); ^{1}H NMR (DMSO-d_6, 400 MHz), δ (ppm): 13.14 (br s, 1H). 11.51 (br s, 1H), 8.56 (d, 1H, J = 2.3 Hz), 8.14 (s, 1H), 8.06 (dd, 1H, J = 8.7, 2.3 Hz), 7.45 (m, 1H), 7.03 (d, 1H, J = 8.6 Hz), 6.95 (m, 1H), 6.41 (m, 1H). ^{13}C NMR (DMSO-d_6, 100 MHz), δ (ppm): 169.6, 144.0, 142.2, 129.6, 129.7, 127.6, 126.1, 122.9, 122.6, 114.1, 114.0, 112.22, 109.4. ESI-MS (m/z) $[M+H]^+$, 253.9.

4.6.4.9. 3-(3,5-Dimethyl-1*H*-pyrrol-2-ylmethylene)-5-nitro-1,3-dihydro-indol-2-one (21). Compound **21** (65% yield); ^{1}H NMR (DMSO-d_6, 400 MHz), δ (ppm): 13.32 (br s, 1H). 11.41 (br s, 1H), 8.75 (d, 1H, J = 2.3 Hz), 8.01 (dd, 1H, J = 8.5, 2.2 Hz), 7.92 (s, 1H), 7.02 (d, 1H, J = 8.6 Hz), 6.08 (bd, 1H, J = 2.4 Hz), 2.36 (s, 3H), 2.34 (s, 3H). ^{13}C NMR (DMSO-d_6, 100 MHz), δ (ppm): 169.8, 142.9, 142.1, 138.4, 134.9, 127.3, 126.8, 126.4, 121.6, 113.8, 113.6, 109.8, 109.0, 13.6, 11.4. ESI-MS (m/z) $[M+H]^+$, 284.0.

4.6.4.10. 3-(1*H*-Indol-3-ylmethylene)-5-nitro-1,3-dihydro-indol-2-one (22). Compound **22** eluted with $CHCl_3$/EtOH/Et_3N (94:5:1) (85% yield); ***Z* Isomer**: ^{1}H NMR (DMSO-d_6, 400 MHz), δ (ppm): 12.17 (br s, 1H), 11.15 (br s, 1H), 9.49 (d, 1H, J = 3.1 Hz), 8.90 (d, 1H, J = 2.2 Hz), 8.53 (s, 1H), 8.34 (m, 1H), 8.07 (dd, 1H, J = 8.3, 2.2 Hz), 7.52 (m, 1H), 7.25 (m, 1H), 7.00 (d, 1H, J = 8.6 Hz). NOESY: dipolar interaction detected between H_4 (δ 8.90) and H_8 (δ 8.53). ^{13}C NMR (DMSO-d_6, 100 MHz), δ (ppm): 168.3, 144.3, 142.0, 136.1, 135.0, 131.5, 128.5, 126.6, 123.0, 122.9, 121.2, 119.1, 116.5, 114.6, 112.4, 111.8, 108.8. EI-HRMS (m/z) $[M]^+$ calcd, 305.0800; obs, 305.0801.

4.6.4.11. 3-(4-Methoxybenzylidene)-5-nitroindolin-2-one (23) (70% yield); *E* isomer. ^{1}H NMR (DMSO-d_6, 400 MHz), δ (ppm): 11.30 (br s, 1H), 8.46 (d, 1H, J = 2.3 Hz), 8.17 (dd, 1H, J = 8.6, 2.3 Hz), 7.78 (part of an AA′BB′ system, 2H, 'J' = 9.0 Hz), 7.78 (s, 1H), 7.13 (part of an AA′BB′ system, 2H, 'J' = 9.0 Hz), 7.05 (d, 1H, J = 8.6 Hz), 3.86 (s, 3H). NOESY: dipolar interaction detected between H_4 (δ 8.46) and H_{10}/H_{14} (δ 7.78). ^{13}C NMR (DMSO, 100 MHz), δ (ppm): 169.1, 161.3, 148.2, 141.5, 139.6, 132.0, 126.2, 126.0, 125.9, 121.5, 117.0, 114.5, 109.9, 55.5. ***Z* Isomer:** ^{1}H NMR (DMSO-d_6, 400 MHz), δ (ppm): 11.30 (br s, 1H), 8.66 (d, 1H, J = 2.3 Hz), 8.54 (part of an AA′BB′ system, 2H, 'J' = 9.1 Hz), 8.16 (s, 1H), 8.13 (dd, 1H, J = 8.6, 2.3 Hz), 7.07 (part of an AA′BB′ system, 2H, 'J' = 9.1 Hz), 6.99 (d, 1H, J = 8.6 Hz), 3.85 (s, 3H). NOESY: dipolar interaction detected between H_4 (δ 8.66) and H_8 (δ 8.16). ^{13}C NMR (DMSO-d_6, 100 MHz), δ (ppm): 167.6, 162.0, 145.6, 142.0, 140.8, 135.2, 126.7, 124.5, 123.7, 121.6, 115.0, 114.0, 109.1, 55.5. ESI-MS (m/z) $[M+H]^+$, 297.3.

4.6.4.12. 3-(4-Diethylamino-benzylidene)-5-nitro-1,3-dihydro-indol-2-one (24) (75% yield); *E* isomer. ^{1}H NMR (DMSO-d_6, 400 MHz), δ (ppm): 11.16 (br s, 1H), 8.60 (d, 1H, J = 2.2 Hz), 8.11 (dd, 1H, J = 8.6, 2.2 Hz), 7.67 (part of an AA′BB′ system, 2H, 'J' = 8.8 Hz), 7.66 (s, 1H), 7.01 (d, 1H, J = 8.6 Hz), 6.80 (part of an AA′BB′ system, 2H, 'J' = 8.8 Hz), 3.45 (q, 4H, J = 6.9 Hz), 1.13 (t, 6H, J = 7.0 Hz). NOESY: dipolar interaction detected between H_4 (δ 8.60) and H_{10}/H_{14} (δ 7.67). ^{13}C NMR (DMSO-d_6, 100 MHz), δ (ppm): 169.7, 149.8, 147.4, 141.4, 140.9, 133.1 (2C), 124.7, 122.4, 119.6, 118.9, 116.3, 111.0 (2C), 109.5, 43.7 (2C), 12.4 (2C). ***Z* isomer**: ^{1}H NMR (DMSO-d_6, 400 MHz), δ (ppm): ^{1}H NMR (DMSO, 400 MHz), δ (ppm): 11.13 (br s, 1H), 8.55 (d, 1H, J = 2.2 Hz), 8.50 (part of an AA′BB′ system, 2H, 'J' = 8.9 Hz), 8.04 (dd, 1H, J = 8.6, 2.3 Hz), 7.97 (s, 1H), 6.94 (d, 1H, J = 8.6 Hz), 6.75 (part of an AA′BB′ system, 2H, 'J' = 8.9 Hz), 3.45 (q, 4H, J = 6.7 Hz), 1.13 (t, 6H, J = 6.8 Hz). NOESY: dipolar interaction detected between H_4 (δ 8.55) and H_8 (δ 7.97). ^{13}C NMR (DMSO-d_6, 100 MHz), δ (ppm): 167.9, 150.3, 144.5, 141.9, 141.8, 136.1 (2C), 127.2, 122.9, 121.2, 116.6, 113.7, 110.7 (2C), 108.6, 43.9 (2C), 12.5 (2C). ESI-MS (m/z) $[M+H]^+$, 338.3.

4.6.4.13. 3-(5-Bromo-furan-2-ylmethylene)-5-nitro-1,3-dihydro-indol-2-one (25). Compound **25** eluted with $CHCl_3$/EtOH (98:2) (75% yield); *E* isomer: ^{1}H NMR (DMSO-d_6, 400 MHz), δ (ppm): 11.30 (br s, 1H), 9.12 (d, 1H, J = 2.3 Hz) 8.20 (dd, 1H, J = 8.6,

2.3 Hz), 7.42 (d, 1H, *J* = 3.5 Hz), 7.41 (s, 1H), 7.03 (d, 1H, *J* = 8.6 Hz), 7.01 (d, 1H, *J* = 3.5). NOESY: detection of the dipolar interaction of H_4 (δ 7.51) hampered by the isochronicity of H_8 (δ 7.41) and H_{11} (δ 7.42). ^{13}C NMR (DMSO-d_6, 100 MHz) δ (ppm): 174.6, 157.4, 153.3, 147.2, 133.4, 131.3, 130.0, 126.5, 125.9, 125.6, 124.8, 121.4, 114.9. ESI-HRMS (*m/z*) $[M+H]^+$ calcd, 333.9589; obs, 333.9580.

4.6.5. General procedure for 5-substituted-3-(1*H*-pyrrol)-1,3-dihydro-indol-2-one, and 5-nitro-3-(5-substituted-3-yl-furan-2-ylmethylene)-1,3-dihydro-indol-2-one by Suzuki cross-coupling

To a stirred solution of the proper boronic acid/ester (0.1 mmol) in dioxane (10 mL), was added a saturated solution of Na_2CO_3 (5 mL), the mixture was degassed and then added [$Pd(P(Ph_3)_4)$] (10 mg). The reaction mixture was heated to 110 °C under argon atmosphere for 12 h, cooled to room temperature and concentrated; CH_2Cl_2 (10 mL) was then added and the solution filtered through Celite. The organic layer was concentrated and the residue was chromatographed on silica gel.

4.6.5.1. 5-Furan-2-yl-3-(1*H*-pyrrol-2-ylmethylene)-1,3-dihydro-indol-2-one (26). Compound **26** eluted with $CHCl_3$/Et_3N (99:1) (65% yield); ^{1}H NMR (DMSO-d_6, 400 MHz), δ (ppm): 13.29 (br s, 1H), 10.99 (br s, 1H), 7.99 (d, 1H, *J* = 1.5 Hz), 7.87 (s, 1H), 7.68 (d, 1H, *J* = 1.5 Hz), 7.47 (dd, 1H, *J* = 8.2, 1.5 Hz), 7.35 (s, 1H), 6.89 (d, 1H, *J* = 8.2 Hz), 6.84 (m, 1H), 6.80 (d, 1H, *J* = 3.3 Hz), 6.55 (m, 1H), 6.35 (m, 1H). ^{13}C NMR (DMSO-d_6, 100 MHz), δ (ppm): 169.3, 153.8, 142.0, 138.4, 129.6, 127.0, 126.0, 125.8, 124.2, 122.4, 120.7, 116.4, 113.9, 112.0, 111.6, 109.8, 104.0. ESI-HRMS (*m/z*) $[M+H]^+$ calcd, 277.0971; obs, 277.0969.

4.6.5.2. 5-(1-Methyl-1*H*-pyrazol-4-yl)-3-(1*H*-pyrrol-2-ylmethylene)-1,3-dihydro-indol-2-one (27). Compound **27** eluted with $CHCl_3$/Et_3N, (99:1) (70% yield); ^{1}H NMR (DMSO-d_6, 400 MHz), δ (ppm): 13.33 (br s, 1H), 10.87 (br s, 1H), 8.03 (s. 1H), 7.87 (d, 1H, *J* = 1.9 Hz), 7.81 (s, 1H), 7.78 (s, 1H), 7.35 (s, 1H), 7.32 (dd, 1H, *J* = 8.3, 2.0 Hz), 6.83 (d, 1H, *J* = 8.2 Hz), 6.80 (m, 1H), 6.35 (m, 3H), 3.48 (s, 3H). ^{13}C NMR (DMSO-d_6, 100 MHz), δ (ppm): 169.3, 137.3, 135.6, 129.6, 127.1, 126.4, 126.1, 125.8, 125.7, 123.7, 122.5, 120.2, 117.0, 115.4, 111.5, 109.8. ESI-HRMS (*m/z*) $[M+H]^+$ calcd, 291.1245; obs, 291.1237.

4.6.5.3. 3-(3,5-Dimethyl-1*H*-pyrrol-2-ylmethylene)-5-furan-3-yl-1,3-dihydro-indol-2-one (28). Compound **28** eluted with $CHCl_3$/Et_3N (99:1) (60% yield); ^{1}H NMR (DMSO-d_6, 400 MHz), δ (ppm): 13.37 (br s, 1H), 10.82 (br s, 1H), 8.11 (m, 1H), 7.97 (d, 1H, *J* = 1.6 Hz), 7.71 (m, 1H), 7.64 (s, 1H), 7.33 (dd, 1H, *J* = 8.0, 1.6 Hz), 6.99 (m, 1H), 6.84 (d, 1H, *J* = 8.0 Hz), 6.01 (d, 1H, *J* = 2.5 Hz), 2.32 (s, 3H), 2.31 (s, 3H). ^{13}C NMR (DMSO-d_6, 100 MHz), δ (ppm): 164.6, 143.9, 138.2, 137.2, 135.9, 131.9, 126.8, 126.5 (2C), 125.0, 123.7, 123.2, 115.5, 112.7, 112.6, 109.5, 109.0, 13.5, 11,4. ESI-HRMS (*m/z*) $[M+H]^+$ calcd, 305.1290; obs, 305.1275.

4.6.5.4. 3-(3,5-Dimethyl-1*H*-pyrrol-2-ylmethylene)-5-pyridin-3-yl-1,3-dihydro-indol-2-one (29). Compound **29** eluted with $CHCl_3$/Et_3N (99:1) (70% yield); ^{1}H NMR (DMSO-d_6, 400 MHz), δ (ppm): 13.37 (br s, 1H), 10.90 (br s, 1H), 8.95 (d, 1H, *J* = 1.8 Hz), 8.50 (d, 1H, *J* = 4.5 Hz), 8.18 (s, 1H), 8.09 (m, 1H), 7.76 (s, 1H), 7.44 (m, 1H), 6.96 (d, 1H, *J* = 8.1 Hz), 6.01 (s, 1H), 2.32 (s, 3H), 2.31 (s, 3H). ^{13}C NMR (DMSO-d_6, 100 MHz), δ (ppm): 169.4, 147.5, 147.3, 137.9, 136.03, 136.0, 133.4, 132.1, 129.8, 126.75, 126.72, 124.1, 123.5, 116.5, 112.5, 112.1, 109.6, 13.4, 11.28. ESI-HRMS (*m/z*) $[M+H]^+$ calcd, 316.1449; obs, 316.1439.

4.6.5.5. 3-[2,3′]Bifuranyl-5-ylmethylene-5-nitro-1,3-dihydro-indol-2-one (30) E isomer. Compound **30** eluting with CH_2Cl_2/AcOEt/*n*-hexane/EtOH (74:20:5:1); (45% yield). ^{1}H NMR (DMSO-d_6, 400 MHz) δ (ppm): 11.30 (br s, 1H), 9.10 (d, 1H, *J* = 2.4 Hz), 8.50 (m, 1H), 8.19 (dd, 1H, *J* = 8.6, 2.3 Hz), 7.89 (m, 1H), 7.50 (d, 1H, *J* = 3.7 Hz), 7.44 (s, 1H), 7.13 (m, 1H), 7.10 (d, 1H, *J* = 3.6 Hz), 7.08 (d, 1H, *J* = 8.7 Hz). NOESY: detected dipolar interaction of H_4 (δ 9.10) with H_{15} (δ 8.50) and H_{17} (δ 7.13). ^{13}C NMR (DMSO-d_6, 100 MHz) δ (ppm): 174.95, 158.00, 154.66, 153.39, 150.35, 146.93, 145.71, 131.31, 130.99, 126.98, 126.36, 123.89, 123.72, 121.80, 115.71, 114.92, 113.12. ESI-HRMS (*m/z*) $[M+H]^+$ calcd, 322.0590; obs, 322.0560.

4.6.5.6. 5-Nitro-3-(5-thiophen-3-yl-furan-2-ylmethylene)-1,3-dihydro-indol-2-one (31) *E* isomer. Compound **31** eluted with CH_2Cl_2/AcOEt/*n*-hexane/EtOH (74:20:5:1) (35% yield); ^{1}H NMR (DMSO-d_6, 400 MHz), δ (ppm): 11.30 (br s, 1H), 9.25 (d, 1H, *J* = 2.3 Hz), 8.31 (dd, 1H, *J* = 2.7, 1.4 Hz), 8.22 (dd, 1H, *J* = 8.7, 2.4 Hz), 7.79 (d, part of AB system, 1H, *J* = 5.1, 2.8 Hz), 7.77 (d, part of AB system, 1H, *J* = 5.1, 1.5 Hz), 7.56 (d, 1H, *J* = 3.8 Hz), 7.49 (s, 1H), 7.24 (d, 1H, *J* = 3.7 Hz), 7.06 (d, 1H, *J* = 8.7 Hz). NOESY: detected dipolar interaction of H_4 (δ 9.25) with H_{15} (δ 8.31) and H_{17} (δ 7.79 or 7.77). ^{13}C NMR (DMSO-d_6, 100 MHz), δ (ppm): 169.7, 155.5, 149.6, 147.8, 141.9, 130.6, 128.2, 126.6, 125.9, 125.3, 122.8, 121.9, 121.4, 118.6, 118.4, 110.4, 109.6. ESI-HRMS (*m/z*) $[M+H]^+$ calcd, 338.0361; obs, 338.0350.

4.6.6. General procedure for 5-amino-3-substituted-1,3-dihydro-indol-2-one

The reaction mixture of the proper 5-nitro-3-substituted-1,3-dihydro-indol-2-one (1 mmol) and $SnCl_2{\cdot}2H_2O$ (10 mmol) in EtOH (8 mL) and 1% HCl (0.08 mL) was heated at 150 °C for 4 h. After cooling to room temperature, the mixture was evaporated and the residue was chromatographed on silica gel, to give the target compounds.

4.6.6.1. 5-Amino-3-(1*H*-pyrrol-2-ylmethylene)-1,3-dihydro-indol-2-one (32). Compound **32** eluted with AcOEt/EtOH/Et_3N (98:1:1) (70% yield); ^{1}H NMR (DMSO-d_6, 400 MHz), δ (ppm): 13.42 (br s, 1H), 10.46 (br s, 1H), 7.28 (s, 1H), 7.28 (m, 1H), 6.81 (d, 1H, *J* = 2.2 Hz), 6.79 (m, 1H), 6.56 (d, 1H, *J* = 8.1 Hz) 6.41 (dd, 1H, *J* = 8.1, 2.2 Hz), 6.30 (m, 1H), 4.66 (br s, 2H). ^{13}C NMR (DMSO-d_6, 100 MHz), δ (ppm): 174.2, 148.6, 135.2, 134.7, 130.9, 130.3, 130.1, 124.8, 123.3, 118.4, 116.3, 115.1, 109.9. ESI-HRMS (*m/z*) $[M+H]^+$ calcd, 226,0980; obs, 226.0966.

4.6.6.2. 5-Amino-3-(3,5-dimethyl-1*H*-pyrrol-2-ylmethylene)-1,3-dihydro-indol-2-one (33). Compound **33** eluted with AcOET/EtOH/Et_3N (98:1:1) (70% yield); ^{1}H NMR (DMSO-d_6, 400 MHz), δ (ppm): 13.38 (br s, 1H), 10.28 (br s, 1H), 7.28 (s, 1H), 6.89 (d, 1H, *J* = 2.0 Hz), 6.56 (d, 1H, *J* = 8.1 Hz) 6.38 (dd, 1H, *J* = 8.1, 2.2 Hz), 5.96 (d, 1H, *J* = 2.2 Hz), 4.53 (s, 2H), 2.30 (s, 3H), 2.26 (s, 3H). NOESY: dipolar interaction detected between H_4 (δ 6.89) and H_8 (δ 7.28). ^{13}C NMR (DMSO-d_6, 100 MHz), δ (ppm): 169.3, 143.2, 134.7, 130.3, 129.6, 126.5, 126.4, 122.0, 114.2, 112.5, 112.1, 109.7, 104.4, 13.5, 11.2. ESI-HRMS (*m/z*) $[M+H]^+$ calcd, 254.1293; obs, 254.1284.

4.6.6.3. 5-Amino-3-(4-methoxybenzylidene)indolin-2-one (34). Compound **34** eluted with CH_2Cl_2/AcOEt/EtOH/Et_3N (77:20:2:1) (70% yield); *E* isomer: ^{1}H NMR (DMSO-d_6, 400 MHz), δ (ppm): 10.07 (br s, 1H), 7.67 (part of an AA′BB′ system, 2H, '*J*' = 8.8 Hz), 7.44 (s, 1H), 7.06 (part of an AA′BB′ system, 2H, '*J*' = 8.8 Hz), 7.02 (d, 1H, *J* = 2.0 Hz), 6.55 (d, 1H, *J* = 8.2 Hz), 6.46 (dd, 1H, *J* = 8.2, 2.0 Hz), 4.67 (br s, 2H), 3.83 (s, 3H). NOESY: dipolar interaction detected between H_4 (δ 7.02) and H_{10}/H_{14} (δ 7.67). ^{13}C

NMR (DMSO-d_6, 100 MHz), δ (ppm): ^{13}C NMR (DMSO-d_6, 100 MHz), δ (ppm): 168.8, 160.2, 143.1, 134.8, 133.2, 131.3, 126.8, 126.7, 121.7, 115.5, 114.2, 110.2, 108.4, 55.3. ***Z* isomer**: ^{1}H NMR (DMSO-d_6, 400 MHz), δ (ppm): 10.12 (br s, 1H), 8.44 (part of an AA′BB′ system, 2H, '*J*' = 8.9 Hz), 7.46 (s, 1H), 7.00 (part of an AA′BB′ system, 2H, '*J*' = 8.9 Hz), 6.87 (d, 1H, *J* = 2.1 Hz), 6.49 (d, 1H, *J* = 8.1 Hz), 6.43 (dd, 1H, *J* = 8.1, 2.1 Hz), 4.55 (br s, 2H), 3.82 (s, 3H). NOESY: dipolar interaction detected between H_4 (δ 7.46) and H_8 (δ 6.87). ^{13}C NMR (DMSO-d_6, 100 MHz), δ (ppm): 167.3, 160.9, 143.1, 135.4, 134.2, 131.2, 127.1, 125.9, 125.3, 114.3, 113.6, 109.6, 105.6, 55.3. ESI-HRMS (*m*/*z*) $[M+H]^+$ calcd, 267.1128; obs, 267.1140.

4.6.6.4. 5-Amino-3-(4-diethylamino-benzylidene)-1,3-dihydro-indol-2-one (35). Compound **35** eluted with CH_2Cl_2/AcOEt/EtOH/Et_3N (77:20:2:1) (70% yield); *E* isomer: ^{1}H NMR (DMSO-d_6, 400 MHz), δ (ppm): 9.96 (br s, 1H), 7.60 (part of an AA′BB′ system, 2H, '*J*' = 9.0 Hz), 7.38 (s, 1H), 7.20 (d, 1H, *J* = 2.2 Hz), 6.74 (part of an AA′BB′ system, 2H, '*J*' = 9.0 Hz), 6.56 (d, 1H, *J* = 8.1 Hz), 6.45 (dd, 1H, *J* = 8.1, 2.2 Hz), 4.85 (br s, 2H), 3.41 (q, 4H, *J* = 7.0 Hz), 1.13 (t, 6H, *J* = 7.0 Hz). NOESY: dipolar interaction detected between H_4 (δ 7.20) and H_{10}/H_{14} (δ 7.60). ^{13}C NMR (DMSO-d_6, 100 MHz), δ (ppm): 169.5, 148.7, 142.5, 136.3, 133.0, 132.2 (2C), 122.8, 122.5, 120.6, 114.7, 110.9 (2C), 109.9, 109.1, 43.8 (2C), 12.5 (2C). ***Z* isomer**: ^{1}H NMR (DMSO-d_6, 400 MHz), δ (ppm): 9.99 (s, 1H), 8,38 (part of an AA′BB′ system, 2H, '*J*' = 9.1 Hz), 7.32 (s, 1H), 6.85 (d, 1H, *J* = 2.2 Hz), 6.69 (part of an AA′BB′ system, 2H, '*J*' = 9.1), 6.50 (d, 1H, *J* = 8.1 Hz), 6.41 (dd, 1H, *J* = 8.1, 2.2 Hz), 4.85 (br s, 2H), 3.41 (q, 4H, *J* = 7.0 Hz), 1.11 (t, 6H, *J* = 7.0 Hz). NOESY: dipolar interaction detected between H_4 (δ 6.85) and H_8 (δ 7.32). ^{13}C NMR (DMSO-d_6, 100 MHz) δ (ppm): 167.7, 149.1, 142.2, 136.6, 134.9 (2C), 130.9, 126.8, 121.5, 121.1, 113.5, 110.5 (2C), 109.2, 105.2, 43.8 (2C), 12.5 (2C). ESI-HRMS (*m*/*z*) $[M+H]^+$ calcd, 308.1762; obs, 308.1762.

4.6.6.5. 5-Amino-3-(5-bromo-furan-2-ylmethylene)-1,3-dihydro-indol-2-one (36) *E* isomer. Compound **36** eluted with CH_2Cl_2/AcOEt/EtOH/Et_3N (77:20:2:1) (70% yield); ^{1}H NMR (DMSO-d_6, 400 MHz), protons H_6 and H_7 are isochronous and with H_4 give rise to a deceptively simple system; δ (ppm): 10.18 (br s, 1H), 7.51 (pseudo t, 1H, '*J*' = 1.4 Hz, H_4), 7.24 (d, 1H, *J* = 3.6 Hz), 7.15 (s, 1H), 6.92 (d, 1H, *J* = 3.6 Hz), 6.60 (pseudo d, 2H, '*J*' = 1.4 Hz, H_6 and H_7), 5.18 (br s, 2H). NOESY: dipolar interaction detected between H_4 (δ 7.51) and H_{11} (δ 7.24). ^{13}C NMR (DMSO-d_6, 100 MHz), δ (ppm): 174.1, 157.9, 139.4, 131.1, 129.1, 126.9, 126.7, 122.7, 121.8, 120.8, 117.0, 115.3, 104.9. ESI-HRMS (*m*/*z*) $[M+H]^+$ calcd, 304.9920; obs, 304.9917.

4.6.6.6. 5-Amino-3-[2,3′]bifuranyl-5-ylmethylene-1,3-dihydro-indol-2-one (37). Compound **37** eluted with CH_2Cl_2/AcOEt/*n*-hexane/EtOH/Et_3N (76:20:3:1) (70% yield); ^{1}H NMR (DMSO-d_6, 400 MHz), protons H_6 and H_7 are isochronous and with H_4 give rise to a deceptively simple system; δ (ppm): 10.20 (broad s, 1H), 8.31 (dd, 1H, *J* = 1.5, 0.9 Hz), 7.85 (t, 1H, *J* = 1.7 Hz), 7.62 (pseudo t, 1H, '*J*' = 1.2 Hz), 7.30 (d, 1H, *J* = 3.7 Hz), 7.21 (s, 1H), 7.01 (dd, 1H, *J* = 1.9, 0.9 Hz), 7.00 (d, 1H, *J* = 3.5 Hz), 6.59 (m, 2H, H_6 and H_7), 4.89 (br s, 2H). NOESY: detected dipolar interaction of H_4 (δ 7.62) with H_{15} (δ 8.31) and H_{17} (δ 7.01). ^{13}C NMR (DMSO-d_6, 100 MHz) δ (ppm): 174.4, 156.2, 155.0, 150.1, 145.1, 138.8, 136.6, 127.7, 127.6, 127.18, 123.3, 121.9, 121.3, 116.6, 115.1, 115.0, 113.3. ESI-HRMS (*m*/*z*) $[M+H]^+$ calcd, 293.0920; obs, 293.0913.

4.6.6.7. *N*-[3-(3,5-Dimethyl-1*H*-pyrrol-2-ylmethylene)-2-oxo-2,3-dihydro-1H-indol-5-yl]-4-(4-methyl-piperazin-1-ylmethyl)-benzamide (38). To a solution of 4-(4-methyl-piperazin-1-yl-methyl)-benzoic acid (50 mg, 0.2 mmol) in DMF (10 mL), DIEA (0.2 mL, 1 mmol) was added at 0 °C. After 10 min, 5-amino-3-(3,5-dimethyl-1*H*-pyrrol-2-ylmethylene)-1,3-dihydro-indol-2-one **(24)** (50 mg, 0.2 mmol), and HBTU (77 mg, 0.2 mmol) were added. The reaction mixture was stirred under argon atmosphere for 12 h and concentrated under reduced pressure. The residue was chromatographed on silica gel and eluted with $CHCl_3$/EtOH/Et_3N, (97:2:1) to give 20 mg (21%). ^{1}H NMR (DMSO-d_6, 400 MHz), δ (ppm): 13.36 (br s, 1H), 10.77 (br s, 1H), 10.08 (br s, 1H), 7.92 (m, 2H), 7.41 (m, 3H), 6.83 (d, 1H), 6.0 (s, 1H), 3.5 (s, 2H), 2.35 (s, 3H), 2.30 (s, 3H), 2.27 (s, 3H), 2.13 (s, 3H). ^{13}C NMR (DMSO-d_6, 100 MHz), δ (ppm): 169.3, 166.4, 143.2, 140.0, 134.7, 130.3, 130.6, 129.8, 129.6, 127.8, 126.5, 126.4, 122.0, 114.2, 112.5, 112.1, 109.7, 104.4, 58.4, 54.5, 52.4, 45.4, 13.5, 11.2. ESI HRMS (*m*/*z*) $[M+H]^+$ calcd, 470.2556; obs, 470.2556.

Acknowledgements

We thank Oriano Marin at University of Padua, Italy, for peptide synthesis; Michela Viltadi, Sara Cazzaniga and Elisa Sala for technical assistance in enzymatic assays; Luca Menilli, Davide Pasin, Pietro Marafini, Camilla Brogiato, Giulia De Biasi and Andrea Mirarco for technical help in compound synthesis. This work was supported by the Italian Association for Cancer Research (AIRC; grant number: IG-4637); the Italian Government MIUR-COFIN program; EU Protein Kinase Research network (Grant number: 503467).

Supplementary data

Supplementary data associated with this article can be found, in the online version, at doi:10.1016/j.bmc.2010.01.011.

References and notes

1. Santoro, M.; Melillo, R. M.; Carlomagno, F.; Vecchio, G.; Fusco, A. *Endocrinology* **2004**, *145*, 5448.
2. Santoro, M.; Carlomagno, F.; Melillo, R. M.; Fusco, A. *Cell. Mol. Life Sci.* **2004**, *61*, 2954.
3. Santoro, M.; Carlomagno, F. *Nat. Clin. Pract. Endocrinol. Metab.* **2006**, *2*, 42.
4. Mologni, L.; Sala, E.; Riva, B.; Cesaro, L.; Cazzaniga, S., et al *Protein Expr. Purif.* **2005**, *41*, 177.
5. Mologni, L.; Sala, E.; Cazzaniga, S.; Rostagno, R.; Kuoni, T., et al *J. Mol. Endocrinol.* **2006**, *37*, 199.
6. Knowles, P. P.; Murray-Rust, J.; Kjaer, S.; Scott, R. P.; Hanrahan, S., et al *J. Biol. Chem.* **2006**, *23*, 23.
7. Mohammadi, M.; McMahon, G.; Sun, L.; Tang, C.; Hirth, P. *Science* **1997**, *276*, 955.
8. Sun, L.; Tran, N.; Tang, F.; App, H.; Hirth, P., et al *J. Med. Chem.* **1998**, *41*, 2588.
9. Rizzi, E.; Cassinelli, G.; Dallavalle, S.; Lanzi, C.; Cincinelli, R., et al *Bioorg. Med. Chem. Lett.* **2007**, *17*, 3962.
10. Sandmeyer, T. *Helv. Chim. Acta* **1919**, *2*, 234.
11. Stamos, J. K. *Synth. Commun.* **1980**, 663.
12. Eguchi, Y.; Ishikawa, M. *Chem. Pharm. Bull. (Tokyo)* **1991**, *39*, 1846.
13. Xu, M.; Wan, P. *Chem. Commun.* **2000**, 2147.
14. Miyaura, N.; Suzuki, A. *Chem. Rev.* **1995**, *95*, 2457.
15. Bellamy, F. D.; Ou, K. *Tetrahedron Lett.* **1984**, *25*, 839.
16. Jackson, S.; DeGrado, W.; Dwivedi, A.; Parthasarathy, A.; Higley, A., et al *J. Am. Chem. Soc.* **1994**, *116*, 3220.
17. Kim, D. W.; Jo, Y. S.; Jung, H. S.; Chung, H. K.; Song, J. H. et al. *J. Clin. Endocrinol. Metab.* **2006**, *91*, 4070. Epub 2006 Jul 4018.
18. Kaminska, J.; Klimczak-Jajor, E.; Skierski, J.; Bany-Laszewicz, U. *Acta Biochim. Pol.* **2008**, *55*, 499.
19. O'Reilly, M. S. *Int. J. Radiat. Oncol. Biol. Phys.* **2007**, *69*, S64.
20. SYBYL 7.3, Tripos International, 1699 South Hanley Rd., St. Louis, Missouri 63144, USA.
21. Moshinsky, D. J.; Bellamacina, C. R.; Boisvert, D. C.; Huang, P.; Hui, T., et al *Biochem. Biophys. Res. Commun.* **2003**, *310*, 1026.
22. Leach, A. R. *Molecular Modelling Principles and Applications*, 2nd ed.; Pearson Prentice Hall, 2001.
23. Lanzi, C.; Cassinelli, G.; Pensa, T.; Cassinis, M.; Gambetta, R. A., et al *Int. J. Cancer* **2000**, *85*, 384.
24. Gunby, R. H.; Sala, E.; Tartari, C. J.; Puttini, M.; Gambacorti-Passerini, C., et al *Anticancer Agents Med. Chem.* **2007**, *7*, 594.
25. Leslie, A. G. W. *Joint CCP4 and ESF-EAMCB Newsletter on Protein Crystallography*, Warrington, UK, 1992.

26. Collaborative computational project The CCP4 suite: programs for protein crystallography. *Acta Crystallogr., Sect. D Biol. Crystallogr.* **1994**, *50*, 760–763.
27. Vagin, A.; Teplyakov, A. *J. Appl. Crystallogr.* **1997**, *30*, 1026.
28. Murshudov, G. N.; Vagin, A. A.; Dodson, E. J. *Acta Crystallogr., Sect. D Biol. Crystallogr.* **1997**, *59*, 1725.
29. Emsley, P.; Cowtan, K. *Acta Crystallogr., Sect. D Biol. Crystallogr.* **2004**, *60*, 2126–2132.
30. Schuettelkopf, A. W.; van Aalten, D. M. F. *Acta Crystallogr.* **2004**, *60*, 1355.
31. Wallace, A.; Laskowski, R.; Thornton, J. *Protein Eng.* **1995**, *8*, 127.